Global Biogeochemical Cycles

RESEARCH ARTICLE
10.1029/2024GB008153

Effects of Mesozooplankton Growth and Reproduction on Plankton and Organic Carbon Dynamics in a Marine Biogeochemical Model

Corentin Clerc[1,2,3], Laurent Bopp[2], Fabio Benedetti[1], Nielja Knecht[1,4], Meike Vogt[1], and Olivier Aumont[3]

[1]Environmental Physics, Institute of Biogeochemistry and Pollutant Dynamics, ETH Zürich, Zürich, Switzerland, [2]LMD/IPSL, Ecole normale supérieure/Université PSL, CNRS, Ecole Polytechnique, Sorbonne Université, Paris, France, [3]LOCEAN/IPSL, IRD, CNRS, Sorbonne Université, MNHN, Paris, France, [4]Stockholm Resilience Center, Stockholm University, Stockholm, Sweden

Key Points:

- Incorporating mesozooplankton growth and reproduction alters carbon cycling pathways, reducing carbon export at 100 m by 10%
- Cohort dynamics lead to significant variations in seasonal dynamics across mesozooplankton size classes without affecting export seasonality
- Statistical predictive models demonstrate consistency between modeled and observed mesozooplankton dynamics globally

Supporting Information:

Supporting Information may be found in the online version of this article.

Correspondence to:

C. Clerc,
corentin.clerc@locean.ipsl.fr

Citation:

Clerc, C., Bopp, L., Benedetti, F., Knecht, N., Vogt, M., & Aumont, O. (2024). Effects of mesozooplankton growth and reproduction on plankton and organic carbon dynamics in a marine biogeochemical model. *Global Biogeochemical Cycles*, *38*, e2024GB008153. https://doi.org/10.1029/2024GB008153

Received 1 MAR 2024
Accepted 25 AUG 2024

Author Contributions:

Conceptualization: Corentin Clerc, Laurent Bopp, Olivier Aumont
Data curation: Corentin Clerc
Formal analysis: Corentin Clerc
Funding acquisition: Laurent Bopp, Meike Vogt, Olivier Aumont
Methodology: Corentin Clerc, Laurent Bopp, Fabio Benedetti, Nielja Knecht, Meike Vogt, Olivier Aumont
Software: Corentin Clerc, Nielja Knecht, Olivier Aumont
Visualization: Corentin Clerc
Writing – original draft: Corentin Clerc

Abstract Marine mesozooplankton play an important role for marine ecosystem functioning and global biogeochemical cycles. Their size structure, varying spatially and temporally, heavily impacts biogeochemical processes and ecosystem services. Mesozooplankton exhibit size changes throughout their life cycle, affecting metabolic rates and functional traits. Despite this variability, many models oversimplify mesozooplankton as a single, unchanging size class, potentially biasing carbon flux estimates. Here, we include mesozooplankton ontogenetic growth and reproduction into a 3-dimensional global ocean biogeochemical model, PISCES-MOG, and investigate the subsequent effects on simulated mesozooplankton phenology, plankton distribution, and organic carbon export. Utilizing an ensemble of statistical predictive models calibrated with a global set of observations, we generated monthly climatologies of mesozooplankton biomass to evaluate the simulations of PISCES-MOG. Our analyses reveal that the model and observation-based biomass distributions are consistent ($r_{pearson}$ = 0.40, total epipelagic biomass: 137 TgC from observations vs. 232 TgC in the model), with similar seasonality (later bloom as latitude increases poleward). Including ontogenetic growth in the model induced cohort dynamics and variable seasonal dynamics across mesozooplankton size classes and altered the relative contribution of carbon cycling pathways. Younger and smaller mesozooplankton transitioned to microzooplankton in PISCES-MOG, resulting in a change in particle size distribution, characterized by a decrease in large particulate organic carbon (POC) and an increase in small POC generation. Consequently, carbon export from the surface was reduced by 10%. This study underscores the importance of accounting for ontogenetic growth and reproduction in models, highlighting the interconnectedness between mesozooplankton size, phenology, and their effects on marine carbon cycling.

1. Introduction

Mesozooplankton are heterotrophic plankton that span a size range of 10^2-10^4 μm and play a central role in marine biogeochemical cycles (Calbet, 2001; Steinberg & Landry, 2017). Mesozooplankton hold an intermediate position in marine trophic webs, as they mediate the energy transfer from phytoplankton and small zooplankton to larger organisms such as fish and large marine mammals (Dupont et al., 2023; Steinberg & Landry, 2017). They regulate the efficiency and intensity of the soft-tissue biological carbon pump (BCP; Steinberg & Landry, 2017; Boyd et al., 2019). Recent model-based studies estimated that mesozooplankton contribute to a quarter of the total carbon sequestered by the BCP (Pinti, DeVries et al., 2023). Due to trophic amplification, mesozooplankton are highly vulnerable to changes in marine ecosystem structure caused by climate change (Chust et al., 2014; Clerc, Aumont, & Bopp, 2023; Kwiatkowski et al., 2019). Hence, quantifying their contribution to biogeochemical processes is key to understanding how changes in mesozooplankton abundance and distribution threaten ecosystem functioning and global biogeochemical cycling. Accurately quantifying the effects of mesozooplankton on ecosystem functions and the carbon cycle necessitates a nuanced understanding of the trade-offs associated with various functional traits exhibited by mesozooplankton, including their feeding mechanisms, life histories, and mortality rates (Hébert et al., 2017; Kiørboe, 2011; Kiørboe et al., 2018; Steinberg & Landry, 2017).

The expression of most plankton functional traits is linked to body size (Andersen et al., 2016; Litchman et al., 2013). Changes in body size throughout the life history of an individual are a primary driver of zooplankton ecology, as body size controls the performance of the "fundamental Darwinian missions" organisms aim to

Writing – review & editing: Corentin Clerc, Laurent Bopp, Fabio Benedetti, Nielja Knecht, Meike Vogt, Olivier Aumont

maximize (feeding, growth, reproduction, and survival; Litchman et al., 2013). In this context, the traits and life histories of mesozooplankton largely differ from those of the smaller microzooplankton, which are mainly composed of protozoans and share many similarities with phytoplankton, except for their trophic mode. Moreover, a significant amount of unicellular marine organisms are mixoplankton (i.e., they can perform both phototrophy and phagotrophy; Mitra et al., 2023), further blurring this trophic distinction. Microzooplankton size variations are generally limited to a doubling or halving of their biovolume, resulting in marginal fluctuations of their metabolic rates throughout their life cycle. On the contrary, mesozooplankton often undergo size changes spanning multiple orders of magnitude. Consequently, these changes in body size contribute to the emergence of distinct phenologies between micro- and mesozooplankton, influencing the seasonality of biogeochemical functions driven by zooplankton. Using a chemostat-like zero-dimensional biogeochemical model, Clerc et al. (2021) showed that a size-based formulation, including explicit reproduction and ontogenetic growth, significantly impacts the seasonal dynamics of mesozooplankton. Indeed, compared to a standard model version in which mesozooplankton are represented as a single and nonvarying size class, the new model version resulted in a delayed response of mesozooplankton to an increase in food availability (i.e., a phytoplankton bloom) by a few months. In addition, mesozooplankton in the new model version started to display cohort dynamics, namely the propagation of successive waves of biomass from small (juvenile) to larger (adult) organisms, controlled by the dependency of the ingestion rate on body size. However, this simplified zero-dimensional framework did not allow for the quantification of the spatial variability of this specific temporal dynamic across different regions of the ocean, nor the corresponding impacts on carbon cycling.

Global models aim to increase the ecological realism in their representation of the marine plankton community. A range of recent global marine ecosystem models now includes the size spectrum of particles (Serra-Pompei et al., 2020), phytoplankton (Blanchard et al., 2014; Heneghan et al., 2020; Serra-Pompei et al., 2020), zooplankton (Heneghan et al., 2020) or even upper trophic levels (Dupont et al., 2023; Maury, 2010). Cohort dynamics are a common emergent pattern in these size spectrum models (Maury et al., 2007; Pope et al., 1994; Zhou et al., 2010). However, the seasonal patterns of the zooplankton size structure are usually not analyzed in such global models, with very few exceptions (e.g., Datta & Blanchard, 2016). In parallel, recent developments in global biogeochemical models have introduced additional zooplankton-related features known to impact the marine biological carbon pump, leading to a better quantification of BCP pathways (Boyd et al., 2019). These features include (a) new functional types, for example: cnidarians (Wright et al., 2021), pelagic tunicates (Clerc, Aumont, & Bopp, 2023; Clerc, Bopp, et al., 2023; Luo et al., 2022), crustacean macrozooplankton (Clerc, Bopp, et al., 2023; Luo et al., 2022) and (b) new processes, for example: diel vertical migration (DVM; Aumont et al., 2018) or grazing parameterization (Rohr et al., 2023). In this context, modeling studies offer a valuable framework for investigating the influence of plankton-mediated pathways on biogeochemical processes. However, existing biogeochemical models often overlook mesozooplankton size variation and reproduction, resulting in a lack of quantification regarding the effects of these processes on carbon cycling (Clerc et al., 2021). One limitation to such an implementation is the difficulty in evaluating mesozooplankton phenology on a global scale due to the sparsity of field observations necessary for model evaluation, even though satellite-based zooplankton indicators are under active development (Basedow et al., 2019; Druon et al., 2019; Strömberg et al., 2009).

In this study, we develop and use PISCES-MOG (Mesozooplankton ontogenetic growth), a new version of PISCES-v2 (Aumont et al., 2015), the standard marine biogeochemistry component of NEMO (Nucleus for European Modelling of the Ocean, Madec, 2008). In PISCES-MOG, mesozooplankton are now represented similarly to Clerc et al. (2021) and the new mesozooplankton module accounts for ontogenetic growth and reproduction. We first explore the global structure of simulated mesozooplankton phenology and characterize the presence and drivers of the emergent cohort dynamics. To evaluate how PISCES-MOG performs in simulating mesozooplankton seasonality, we derive a global mesozooplankton monthly climatology by training an ensemble of biomass distribution models (BDMs) based on the MAREDAT mesozooplankton biomass data set (Moriarty & O'Brien, 2013) in combination with the recent predictive modelling framework of Knecht et al. (2023). We also evaluate the skill of PISCES-MOG in reproducing the seasonal patterns in mesozooplankton size-structure by comparing the model-based seasonal cycles to those observed at two well-studied time series: the Hawaii ocean time series (HOT; Sheridan & Landry, 2004), and the Bermuda Atlantic time series study (BATS; Steinberg et al., 2001). We then investigate how the simulated cohort dynamics affect the biogeochemical properties of the total mesozooplankton to answer the following questions: Does the inclusion of ontogenetic growth and reproduction induce a change in mesozooplankton seasonality and biomass distribution, compared to that simulated by

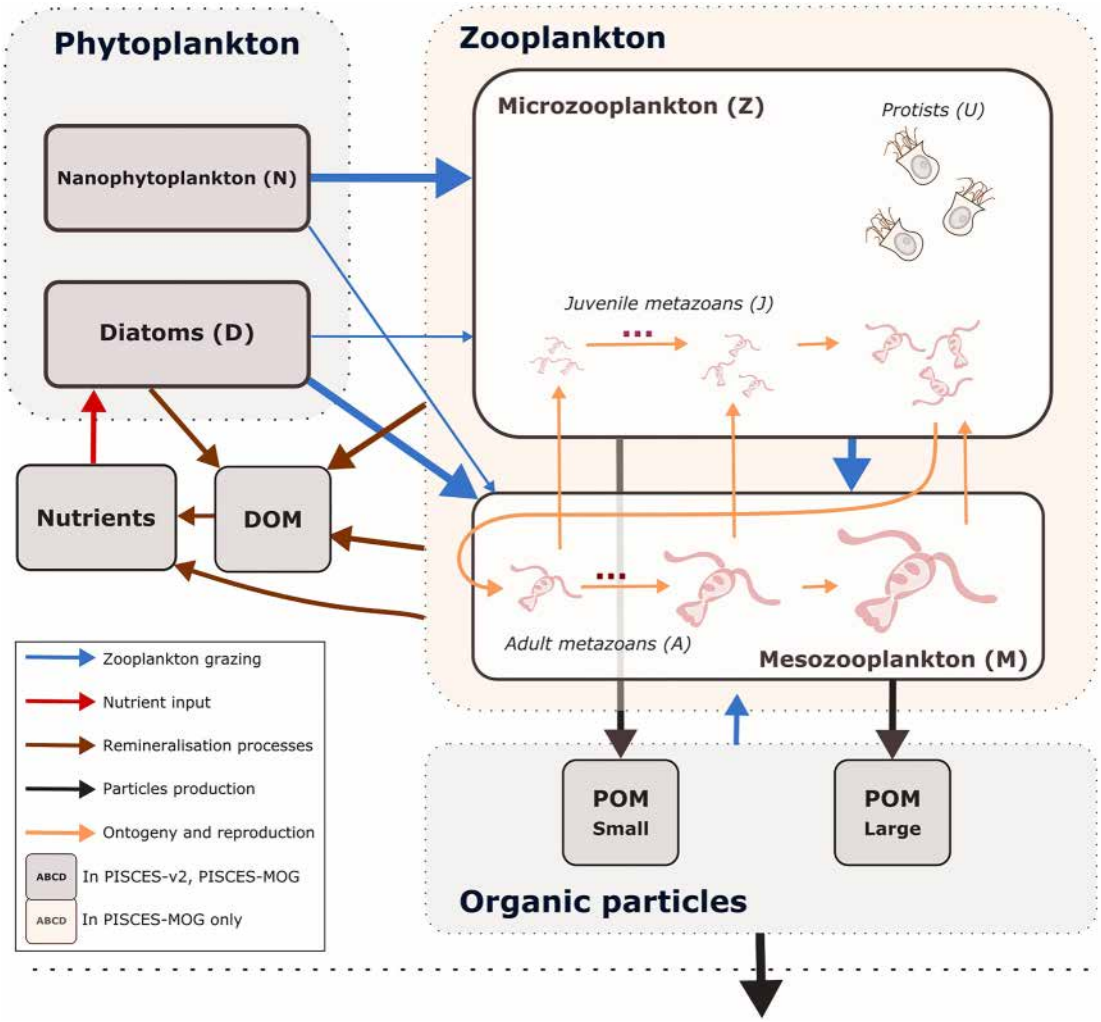

Figure 1. Architecture of the PISCES-MOG (mesozooplankton ontogenetic growth) model in the study. This figure illustrates the living and non-living organic components of the model (boxes) and their interactions (arrows). This diagram emphasizes trophic interactions (i.e., blue arrows, the width representing the preference of the predator for the prey) as well as particulate organic matter production (i.e., black arrows), two processes impacted by the introduction of metazoan reproduction (vertical upward orange arrows) and ontogenetic growth (other orange arrows) in PISCES-MOG. POM = Particulate Organic Matter; DOM = Dissolved Organic Matter.

a model with a single and nonvarying size representation (as in PISCES-v2)? Does this affect the phenology and distribution of other living and non-living particle components, and how do all these factors influence the carbon fluxes associated with the BCP?

2. Materials and Method

2.1. Model Description

2.1.1. Model Structure

The marine biogeochemical model used in the present study is a revised version of PISCES-v2 (gray boxes in Figure 1, Aumont et al., 2015). It includes five nutrient pools (Fe, NH_4^+, Si, PO_4^{3-} and NO_3^-), two phytoplankton groups (Diatoms and Nanophytoplankton, denoted D and N), two zooplankton size classes (Micro- and Meso-zooplankton, denoted $\mathcal{Z}$ and $\mathcal{M}$) and an explicit representation of dissolved and particulate organic matter, reaching a total of 24 prognostic variables (tracers). A full description of the model is provided in Aumont et al. (2015).

Since multicellular zooplankton grow in size during their life, in PISCES-MOG, the microzooplankton and mesozooplankton compartments have been modified to explicitly represent a single community of metazoan

Table 1
Parameters and Equations Used in the Size-Based Parameterizations

Term	Value	Description
$l_{\min}$		Minimal metazoan zooplankton body length
$l_{\max}$		Maximal metazoan zooplankton body length
v	$= \frac{N_S}{3 \ln \frac{l_{\max}}{l_{\min}}}$	Transition rate between the mesozooplankton size-classes
$g_{\mathcal{M}}^{\max}$		Geometric mean of the maximum adult metazoans ingestion rate
$g_{\mathcal{Z}}^{\max}$		Geometric mean of the maximum juveniles metazoans ingestion rate
$L(J_s)$	$= \frac{2s+1}{2N_S}$	Length factor of juvenile size-classes J_s
$L(A_s)$	$= \frac{N_s+2s+1}{2N_S}$	Length factor of adult size-classes A_s
$L(U)$	$= \frac{1}{4}$	Length factor for generic microzooplankton U
$\ln g_s^{\max}$	$= \ln g_{\mathcal{Z}}^{\max} + \alpha(L(U) - L(X_s)) \ln\left(\frac{l_{\max}}{l_{\min}}\right)$	Maximum ingestion rate of the zooplankton size-class X_s
$\ln m_s$	$= \ln m_{\mathcal{Z}} + \alpha(L(U) - L(X_s)) \ln\left(\frac{l_{\max}}{l_{\min}}\right)$	Quadratic mortality rate of the zooplankton size-class X_s

Note. To parameterize size in the equations, we introduce a length factor L for each size class. It ranges from 0 (minimum length) to 1 (maximal length) and varies linearly with the logarithm of the length.

individuals that grow in size and reproduce. To achieve this, PISCES-MOG includes a subdivision of the zooplankton to represent different metazoan size classes, mesozooplankton sexual reproduction, and ontogenetic growth. Zooplankton representation in PISCES-MOG has been updated from PISCES-v2 based on the size-structured model outlined in Clerc et al. (2021) (Figure 1).

In PISCES-MOG, we consider a subdivision of the metazoan zooplankton into N_s size classes of equal width in logarithmic space. The center of each size class is defined as follows: $l_s = l_{\min}\left(\frac{l_{\max}}{l_{\min}}\right)^{\frac{2s+1}{2N_s}}$ where $s \in [0,\ N_s - 1]$. The width of each size class is $\Delta\ln(l_s) = \frac{1}{N_s}\ln\left(\frac{l_{\max}}{l_{\min}}\right)$ in logarithmic space and is therefore constant. Microzooplankton $\mathcal{Z}$ is now divided into strictly heterotrophic protists U and the $\frac{N_s}{2}$ first metazoan size classes, representing juvenile metazoan zooplankton, J_i with $i \in \left[0,\ \frac{N_s}{2} - 1\right]$. The remaining $\frac{N_s}{2}$ size classes, representing adult metazoan zooplankton, A_i with $i \in \left[0,\ \frac{N_s}{2} - 1\right]$, form the mesozooplankton compartment $\mathcal{M}$ in PISCES-MOG. The adult metazoan size class of maximum size is denoted as $A_{\max}$.

2.1.2. Metazoans and Heterotrophic Protists Dynamics

We first describe zooplankton dynamics using five equations corresponding to the smallest juveniles (Equation 1), the other juveniles (Equation 2), the smallest adults (Equation 3), the other adult metazoan size classes (Equation 4), and the heterotrophic protists (Equation 5). For readability, in all equations, the same symbol will be used to represent both a zooplankton group (when it appears as an index or exponent) and its concentration.

For any zooplankton group X, G_X represents grazing, while m_X and r_X represent quadratic and linear mortalities (Equations 1–5). $g_{\mathcal{M}}^{\mathcal{Z}}$ is the rate of microzooplankton ingestion by mesozooplankton (Equations 1, 2 and 5). Similarly to (Clerc et al., 2021), for each adult mesozooplankton A_s, part of the assimilated food w is allocated to reproduction and is transferred to the juvenile subcompartment J_s (Equations 1–4). This representation assumes that we represent a community of metazoan individuals with a constant egg-to-adult ratio. The remainder of the assimilated food is used for growth, resulting in a transfer between adjacent size classes at a rate v (Equations 1–4). The value of this parameter depends on the number of size classes and the assumed size distribution within each size class (see Table 1 and Clerc et al., 2021). For the largest size class of adult mesozooplankton $A_{\max}$, no size growth is possible.

Thus, the equations describing juvenile metazoan dynamics are:

$$\frac{\partial J_0}{\partial t} = \left[\underbrace{(1-v)G_{J_0}}_{\text{growth and transition}} - \underbrace{g^{\mathcal{Z}}_{\mathcal{M}}\mathcal{M}}_{\text{predation}} - \underbrace{m_{A_0}\mathcal{Z} - r_{J_0}}_{\text{mortality}} \right] \cdot J_0 + \underbrace{wG_{A_0}A_0}_{\text{reproduction}} \tag{1}$$

$$\frac{\partial J_s}{\partial t} = \left[\underbrace{(1-v)G_{J_s}}_{\text{growth and transition}} - \underbrace{g^{\mathcal{Z}}_{\mathcal{M}}\mathcal{M}}_{\text{predation}} - \underbrace{m_{J_s}\mathcal{Z} - r_{J_s}}_{\text{mortality}} \right] \cdot J_s + \underbrace{vG_{J_{s-1}}J_{s-1}}_{\text{transition}} + \underbrace{wG_{A_s}A_s}_{\text{reproduction}} \tag{2}$$

And the equations describing adult metazoan dynamics are:

$$\frac{\partial A_0}{\partial t} = \left[\underbrace{(1-w)(1-v)G_{A_0}}_{\text{growth, reproduction and transition}} - \underbrace{m_{A_0}\mathcal{M} - r_{A_0}}_{\text{mortality}} \right] \cdot A_0 + \underbrace{vG_{J_{\frac{N_s}{2}-1}}J_{\frac{N_s}{2}-1}}_{\text{transition}} \tag{3}$$

$$\frac{\partial A_s}{\partial t} = \left[\underbrace{(1-w)(1-v)G_{A_s}}_{\text{growth, reproduction and transition}} - \underbrace{m_{A_s}\mathcal{M} - r_{A_s}}_{\text{mortality}} \right] \cdot A_s + \underbrace{(1-w)vG_{A_{s-1}}A_{s-1}}_{\text{transition}} \tag{4}$$

Heterotrophic protists, U, follow the same dynamics as microzooplankton in PISCES-v2, except for predation by mesozooplankton and quadratic mortality which are now scaled to the full PISCES-MOG microzooplankton compartment ($\mathcal{Z} = U + \sum J$) to keep equivalency between PISCES-v2 and PISCES-MOG microzooplankton compartments.

$$\frac{\partial U}{\partial t} = \left[\underbrace{G_U}_{\text{growth}} - \underbrace{g^{\mathcal{Z}}_{\mathcal{M}}\mathcal{M}}_{\text{predation}} - \underbrace{m_U\mathcal{Z} - r_U}_{\text{mortality}} \right] \cdot U \tag{5}$$

Overall, unicellular heterotrophic protists and juvenile metazoans aim to represent the same community as microzooplankton in PISCES-v2 and adult metazoan groups aim to represent the same community as mesozooplankton in PISCES-v2, for which the parameterization is mainly based on copepods (Aumont et al., 2015). Thus, the temporal evolution of the N_s metazoan zooplankton groups is computed according to PISCES-v2 micro- and mesozooplankton equations, except the newly introduced ontogenetic growth and reproduction terms (derived from Clerc et al., 2021). Consequently, for the zooplankton group X, grazing (G_X), quadratic (m_X) and linear mortalities (r_X) parameterizations are identical to that of micro- and mesozooplankton in PISCES-v2:

$$G_X = e^X g_X (1 - \Delta(O_2)) f_X(T) \tag{6}$$

$$r_X = r^0_X f_X(T) \left(\frac{X}{K_m + X} + 3\Delta(O_2) \right) \tag{7}$$

$$m_X = m^0_X f_X(T)(1 - \Delta(O_2))\, X^2 \tag{8}$$

In Equation 6, g_X is the total ingestion rate, defined as in Equations 24 and 28 in Aumont et al. (2015). All zooplankton groups feed on diatoms, nanophytoplankton, and small POC. In addition, mesozooplankton feed on heterotrophic protists, juveniles, and large POC. Food preferences (blue arrow thickness in Figure 1) are constant for each major zooplankton compartment (microzooplankton and mesozooplankton). For mesozooplankton, in addition to conventional suspension feeding based on a Michaelis-Menten parameterization without switching

and a threshold, flux feeding (Jackson, 1993; Stukel et al., 2019) is also represented (Equations 29a and 29b in Aumont et al., 2015). e^X is the growth efficiency.

All terms in Equations 6–8 were given the same temperature sensitivity $f_X(T)$, where T is temperature, using a Q10 of 2.14 (Equations 25a and 25b in Aumont et al., 2015), as for mesozooplankton in PISCES-v2 and according to Buitenhuis et al. (2006). Growth rate and quadratic mortality are reduced and linear mortality is enhanced at very low oxygen levels, as we assume that mesozooplankton are not able to cope with anoxic waters ($\Delta(O_2)$, where O_2 is dissolved oxygen concentration, is an anoxia parameterization that varies between 0 in fully oxic conditions and 1 in fully anoxic conditions, see Equation 57 in Aumont et al., 2015). Linear mortality is also enhanced at high organism concentrations (K_m is the half-saturation constant for mortality, Equation 8). m_X^0 (Equation 7) and r_X^0 (Equation 8) are the quadratic and linear mortality rates at 0°C in oxic conditions.

All of the other 22 biogeochemical tracers that are common to PISCES-v2 and PISCES-MOG are driven by the exact same equations, which are fully detailed in Aumont et al. (2015).

2.1.3. Size-Based Parameterization

The maximum ingestion rates of the different zooplankton classes are set according to the allometric relationship proposed by Hansen et al. (1997). We assumed that the same allometric relationship applies to quadratic mortality rates, although this assumption is not explicitly supported by Hansen et al. (1997). The half-saturation constant used in the grazing parameterization is supposed constant as observations suggest no significant variations with size (Hansen et al., 1997). The transition rate v between the different size classes was computed analytically by assuming that the slope of the normalized biomass size spectrum within each size class is constant in a log-log space (see Supporting Information S1 in Clerc et al., 2021). It is set to -1 following the seminal study of Sheldon et al. (1972), which corresponds to an approximate constant biomass in logarithmically equal size intervals. The expressions for the transition rate and for the maximum ingestion rate are shown in Table 1. The size-dependent formulations used in our standard model configuration are also listed in Table 1.

2.2. Numerical Experiments

2.2.1. Reference Simulation

PISCES-MOG is run in offline mode with dynamic fields identical to those used in Aumont et al. (2015). These climatological dynamic fields (as well as the input files) can be obtained at www.nemo-ocean.eu and were produced using an ORCA2-LIM configuration (Madec, 2008). The spatial resolution is about 2° by $2°\cos(\phi)$ (where ϕ is the latitude) with a meridional resolution enhanced to 0.5° at the equator. The model has 30 vertical layers with increasing vertical thickness from 10 m at the surface to 500 m at 5,000 m. PISCES-MOG was initialized from the quasi-steady-state simulation presented in Aumont et al. (2015). N_S, the number of metazoan size classes was set to 20 to achieve a reasonable discretization of a metazoan size-spectrum while limiting the computational cost to a doubling compared to PISCES-v2. Thus, microzooplankton include 10 juvenile metazoan size classes and one heterotrophic protist size class. Mesozooplankton include 10 adult metazoan size classes. The size parameterization defines metazoans in the model as a community of individuals ranging from 10 to 4,000 µm, which implies a mean egg-to-adult body length ratio of 1/20. An upper size range of 4,000 µm was chosen to account for large copepod species like *Calanus hyperboreus* while maintaining a reasonable egg-to-adult body length ratio, which is in the lower range of the ratios documented in Brun et al. (2017). The initial concentrations of the 21 zooplankton groups were set to a small uniform value of 10^{-3} mmol C m^{-3}. The model was then integrated for the equivalent of 100 years, forced with 5-day averaged ocean dynamic fields and with a 3-hr integration time step. All the analyses are performed on the last year of the simulation. When not specified, the parameter values are identical to those of PISCES-v2 (Aumont et al., 2015). The other parameter values are given in Table 2.

2.2.2. Sensitivity Experiments

To investigate the influence of each new mesozooplankton feature (e.g., reproduction, ontogenetic growth, and size structure) on the model's behavior, we conducted sensitivity experiments based on three alternative model versions. The resulting biogeochemical model properties are compared with those of the standard model, PISCES-MOG.

Table 2
Parameter Values of the Default Configuration

Parameter	Default	Unit	Description	Range	Source
N_S	20	–	Number of mesozooplankton size-classes		
$g_{\mathcal{M}}^{\max}$	0.5	d^{-1}	Geometric mean of the maximum adult metazoans ingestion rate	0.13–0.97	(Buitenhuis et al., 2006)
$g_{\mathcal{Z}}^{\max}$	2.0	d^{-1}	Geometric mean of the maximum juveniles metazoans ingestion rate	0.55–4.1	See Table 1
$m_{\mathcal{M}}^{0}$	1.5×10^{-2}	$m^3\ mmol^{-1}\ d^{-1}$	Geometric mean of adult metazoans quadratic mortality		(Aumont et al., 2015)
$m_{\mathcal{Z}}^{0}$	5.0×10^{-3}	$m^3\ mmol^{-1}\ d^{-1}$	Geometric mean of juveniles metazoans quadratic mortality		See Table 1
w	0.3	–	Fraction of the assimilated food allocated to reproduction	0.2–0.8	(Kooijman, 2013)
v	1.1	–	Transition rate across metazoan size-classes		(Clerc et al., 2021)
$l_{\min}$	10	μm	Minimal metazoan zooplankton body length		
$l_{\max}$	4,000	μm	Maximal metazoan zooplankton body length		
α	0.48	–	Allometric parameter	0.42–0.54	(Hansen et al., 1997)

The first alternative model version simply corresponds to the PISCES-v2 standard model. Here, metazoans are represented by a single mesozooplankton compartment, while the microzooplankton only include one heterotrophic protist size class. Thus, juvenile and adult metazoan organisms are assumed to have the same metabolic rates and the same predation behavior. In this model, the representation of both microzooplankton and mesozooplankton is similar and corresponds to a formalism used for heterotrophic protists whose reproduction mode is based on cell division. This model serves as a reference representing the most common mesozooplankton formulation in the biogeochemical components of Earth System Models (Kearney et al., 2021).

In the second alternative model version, PISCES-MOG-2LS ("Two-life-stage"), the representation of metazoan zooplankton is limited to two size classes: juveniles and adult organisms (microzooplankton include one juvenile metazoan size class and one heterotrophic protist size class; mesozooplankton include one adult metazoan size class only). As a result, the computing cost of PISCES-MOG-2LS is reduced by a factor of two compared to PISCES-MOG. PISCES-MOG-2LS was built to investigate the effect of a full-size spectrum representation of metazoans (in PISCES-MOG but not in PISCES-MOG-2LS) on the spatiotemporal dynamics of the system.

In the third alternative model version, PISCES-MOG-CM ("Constant Mortality"), zooplankton compartmentation is identical to the one in PISCES-MOG, but quadratic mortality rates are constant across all size classes of each zooplankton compartment. Indeed, in the chemostat-like model presented in Clerc et al. (2021), the allometric scaling was only applied to maximum ingestion rates and not to quadratic mortality rates. Thus, PISCES-MOG-CM serves as a reference representing the zooplankton dynamics from Clerc et al. (2021)'s model. The resulting system dynamics are very similar to those of PISCES-MOG and subsequently will not be presented in this paper. A figure comparing PISCES-MOG and PISCES-MOG-CM outputs is available in the (Figures S1 and S2 in Supporting Information S1).

2.2.3. Metrics to Evaluate the Seasonality of Different Plankton Functional Groups

Given the high dimensionality of the biomass outputs of PISCES-MOG (space, time, and size), summary metrics are needed to describe the global metazoan seasonality. To this end, we designed a set of four phenological metrics inspired by (Llort et al., 2015): (a) Relative Seasonal Amplitude is computed as the difference between the annual minimal and maximal biomass, normalized by the yearly average. (b) Bloom Apex refers to the time of year when biomass reaches its maximum. (c) Bloom Climax refers to the time of year when population growth (derivative of the biomass) is maximal. (d) Bloom duration is defined as the total period during which biomass is equal to or higher than a threshold and indicates the length of the bloom period. The threshold value is calculated as $B_{\min} + 0.75 \times (B_{\max} - B_{\min})$, where $B_{\min}$ and $B_{\max}$ are the annual minimal and maximal biomasses.

2.3. Observations-Based Products

We used two distinct observations-based products for model evaluation: (a) a global monthly climatology of mesozooplankton biomass was used to evaluate how the model performs in simulating the seasonality of global mesozooplankton distribution (Moriarty & O'Brien, 2013), and (b) monthly climatologies from local time series

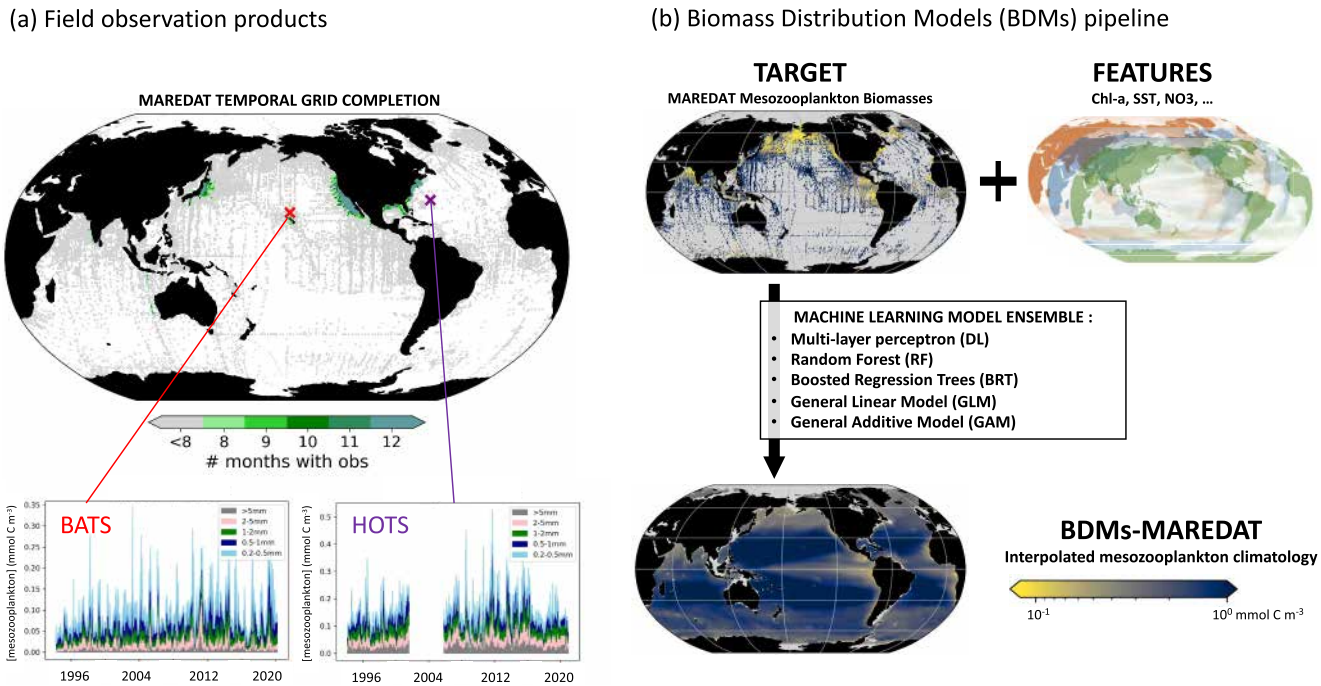

Figure 2. Description of the fields observation and biomass distribution models (BDMs) data sets. (a) Spatio-temporal coverage of mesozooplankton biomass field observations from MAREDAT global monthly climatologies (Moriarty & O'Brien, 2013) and from the BATS and HOT time-series stations (Sheridan & Landry, 2004; Steinberg et al., 2001) (b) BDMs pipeline trained on the MAREDAT monthly climatology of mesozooplankton biomass integrated over the top 200 m (Moriarty & O'Brien, 2013).

are used to evaluate the model performance in reproducing the size-structure of mesozooplankton biomass and seasonality (Sheridan & Landry, 2004; Steinberg et al., 2001).

2.3.1. Global Mesozooplankton Monthly Climatology

To be able to compare the mesozooplankton biomass distribution simulated by PISCES-MOG to observational data, we use a new habitat modeling pipeline for continuous target variables (Knecht et al., 2023). This pipeline enabled us to estimate monthly fields of mesozooplankton biomass in model units of mmol C m^{-3} for the global epipelagic ocean. To do so, we relied on observational monthly mesozooplankton biomass fields from MAREDAT (the MARine Ecosystem DATa; Moriarty & O'Brien, 2013) in combination with climatological fields of the environmental predictors of mesozooplankton biomass (Benedetti et al., 2021; Knecht et al., 2023; Strömberg et al., 2009).

MAREDAT mesozooplankton biomass product. The MAREDAT mesozooplankton biomass field consists of 153,163 field measurements of mesozooplankton biomass concentrations and was extracted from the Coastal and Oceanic Plankton Ecology, Production, and Observation Database (COPEPOD; http://www.st.nmfs.noaa.gov/copepod). These measurements were quality controlled, standardized across different sampling and measurement methods and then aggregated into global climatological biomass concentration values. More information about the treatment and standardization of data in COPEPOD are available in O'Brien (2010) and in Moriarty and O'Brien (2013). After re-gridding, the MAREDAT biomass fields comprise 42,245 data points on the WOA grid (1° × 1° × 12 months × 33 depths), expressed in mmol C m^{-3} (Moriarty & O'Brien, 2013). In our study, these standardized monthly values are vertically integrated between 0 and 200 m to be representative of the epipelagic zone which is where most of the zooplankton organisms are concentrated. The resulting climatology encompasses 27% of the epipelagic ocean area and shows an uneven distribution between the hemispheres. The spatial coverage is 40% in the northern hemisphere and 16% in the southern hemisphere. Moreover, the data set has limited temporal coverage, as only 1% of the grid cells contain data for at least 8 distinct months (i.e., including observations that span at least three seasons), mostly concentrated near the coasts of Japan and the US (Figure 2a). To address this spatiotemporal bias, we employ an ensemble of statistical data-driven models to predict

mesozooplankton biomass concentration as a function of biologically relevant environmental predictors and map it onto a global monthly 1° × 1° grid (Knecht et al., 2023). Such a statistical modeling framework is widely used in community ecology and biogeography to predict the spatial distribution of species and emerging diversity patterns based on environmental covariates (Melo-Merino et al., 2020). In our study, we adapt the concept of species distribution modeling to model mesozooplankton biomass as a continuous target variable (as opposed to the binary presence-absence data commonly used in the fields of community ecology and biogeography, Guisan & Zimmermann, 2000; Elith & Leathwick, 2009; Righetti et al., 2019; Benedetti et al., 2021; Waldock et al., 2022).

Biomass Distribution Models (BDM)-ensemble. We used the ensemble of monthly climatologies of environmental variables from Knecht et al. (2023) to identify the set of potential environmental predictors that explain a substantial variance in the biomass data, in order for these predictors to be used in training the BDMs. These climatologies were selected as potentially relevant for modeling the biomass of pteropods and foraminifers, two important mesozooplankton functional groups that share similar predictors with copepods (Benedetti et al., 2023). Where necessary, these environmental predictor fields were averaged and re-gridded to monthly climatologies on a 1° × 1° resolution. We followed a similar approach as described in (Knecht et al., 2023) to select the set of predictors used in training the BDMs. Initially, using univariate Generalized Additive Models (GAM) and Generalized Linear Models (GLM), we evaluated the percentage of deviance explained by each selected predictor at various spatial aggregation levels (Knecht et al., 2023). We retained all predictors that explained 5% of the variability at any of the spatial aggregation levels. We used a Pearson correlation coefficient threshold ($|r| \geq 0.7$) to identify clusters of collinear variables, which cannot reliably be discerned by our statistical models (Dormann et al., 2013). Then, we used univariate tests to identify the predictor displaying the highest predictive skill within those collinearity clusters. These top-ranking predictors were selected to represent all the candidate predictors in the cluster to which they belong. The resulting set of predictors includes surface chlorophyll-*a*, mixed layer depth (MLD), nitrate concentrations averaged over the MLD, partial pressure of CO_2, total alkalinity, eddy kinetic energy (EKE) and photosynthetically active radiation (PAR). Note that chlorophyll-*a*, EKE, MLD and nitrate concentration were log-transformed, so their distribution is closer to a Gaussian distribution. The final set of predictors is consistent with the predictors that were retained to model global zooplankton habitat suitability patterns in other SDM-based studies (Benedetti et al., 2021; Knecht et al., 2023; Strömberg et al., 2009).

We trained an ensemble of five BDMs with the selected environmental predictor variables and gridded, depth-integrated mesozooplankton biomass, using a 75%:25% train-test split and five-fold cross-validation following the method detailed in Knecht et al. (2023). The five BDMs include a GLM, a GAM, a Random Forest (RF), a Gradient Boosting Machine (GBM), and a Neural Network/Deep Learning Model (DL; see Figure 2b). Model parameter tuning for the RF, GBM, and DL was performed using grid search (see Table S2 in Supporting Information S1 for the list of tuned hyperparameters). The statistical modeling framework was conducted in the R coding environment (R Core Team, 2022) based on the h2o 3.36.0.3 R package (H2O.ai, 2021).

We applied the BDMs to predict monthly mesozooplankton biomass values for the epipelagic layer globally. These projections were made for each grid cell and month with available data for all the predictors included in the BDMs. Statistical predictive models including too many complex features can suffer from limited transferability into novel environmental conditions due to non-linear response curves (Bell & Schlaepfer, 2016; Elith et al., 2010; Qiao et al., 2019). To address this issue, we evaluated whether the environmental conditions for each grid cell fell within the range of the training data set or were non-analogue states, using a Multivariate Environmental Similarity Surfaces (MESS) analysis (Elith et al., 2010). This allows us to flag those locations of the ocean where our spatial predictions of mesozooplankton biomass are more uncertain due to model extrapolation into non-analogue conditions.

We assessed the performance of each BDM based on three metrics. The root mean squared error (RMSE) is an error metric estimating the deviation between predicted and true values. The coefficient of determination, R^2, indicates the magnitude of correspondence between trends in the predicted and observed values. Finally, the Nash-Sutcliffe efficiency (NSE; Nash & Sutcliffe, 1970) compares the model performance to a null model, that is, the mean of all observations. Positive NSE values indicate that the assessed model performs better than the null model. Each performance metric was calculated on both the training and the testing set of the data. The models perform reasonably well (Table S1 in Supporting Information S1), with the RF model showing the best performance across all metrics (RMSE = 0.22, R^2 = 0.52, NSE = 0.52 on the test set), followed by the GBM and then the DL model. Chlorophyll-*a* concentration was found to be the most important predictor as it explains 42.1%

Table 3
Evaluation Metrics Computed to Compare the Model-Based and the Observation-Based Mesozooplankton Biomass Monthly Climatologies

	Comparison			Mean		Standard deviation	
	Corr	RMSE	Bias	Obs.	Model	Obs.	Model
Average biomass (mmol C m^{-3})	0.40	0.14	0.09	0.18	0.27	0.10	0.11
Bloom apex (days)	0.25	75	−15	158	144	57	56
Bloom climax (days)	0.32	77	0	87	87	60	57
Bloom duration (days)	0.04	50	14	75	89	37	32
Relative amplitude (%)	0.52	42%	−3%	82%	79%	43%	46%

Note. Obs refers to the BDMs-MAREDAT product, Model here refers to the PISCES-MOG mesozooplankton outputs. With the exception of correlation coefficients, metric units are the same as the units of the evaluated variable. Corr is the correlation coefficient between the BDM-based and the PISCES-MOG-based fields of mesozooplankton biomass. For the average concentration, the bloom duration and the relative amplitude, the metric corresponds to the Pearson correlation coefficient. For the bloom climax and bloom apex, the metric corresponds to the circular version of the Pearson correlation coefficient (Jammalamadaka & SenGupta, 2001), since those are periodic metrics (with a period of 1 year). The periodicity of those metrics is also accounted for in the computation of root mean square error (RMSE) and Bias. All metrics are weighted by the area of each ocean grid cell and averaged over the top 200 m of the ocean. Seasonality metrics are also weighted. Note that a visualization of the comparison between PISCES-MOG and BDMs-MAREDAT mesozooplankton metrics is available in Figure S13 in Supporting Information S1.

of the model's predictive power on average. This finding supports the models' ability to capture the responses of zooplankton biomass to large-scale gradients of plankton productivity (Strömberg et al., 2009). The supplementary materials include annually averaged mesozooplankton biomass maps for the five models, seasonal maps, and the Partial Dependency Plots (PDP) that show the response learnt by the BDMs to the gradients of predictors included (Figures S3, S4, and S5 in Supporting Information S1).

To evaluate the global mesozooplankton biomass of PISCES-MOG, model outputs were vertically integrated over the top 200 m and horizontally re-gridded to match the grid of the BDMs predictions. Then, annually averaged fields were computed and PISCES-MOG outputs were compared against the BDM outputs based on relevant quantitative statistics (see Table 3).

2.3.2. Size-Structured Mesozooplankton Climatologies at BATS and HOT

To compare the size-specific seasonal dynamics of metazoan simulated by PISCES-MOG to in situ observations, we used two widely studied time series of size-structured mesozooplankton biomass, the Hawaii ocean time series (HOT; Sheridan & Landry, 2004) and the Bermuda Atlantic time series (BATS; Steinberg et al., 2001). Mesozooplankton at HOT and BATS have been collected biweekly to monthly since 1994 at day time and night time through two replicate oblique net tows equipped with a 200 µm mesh net, in the top 200 m of the water column. The samples were divided into two halves, and one half underwent successive wet sieving with nested sieves of various mesh sizes (5.0, 2.0, 1.0, 0.5, and 0.2 mm). The resulting fractions were placed on nets with a 0.2 mm mesh size, frozen, thawed, blotted, and then analyzed for dry weight on shore (Madin et al., 2001). Thus, dry weight mesozooplankton time series, in mg m^{-2}, are available for five size classes: 0.2–0.5, 0.5–1, 1–2, 2–5, and >5 mm. We downloaded the 1994–2019 mesozooplankton biomass times series at *bats.bios.asu.edu* for BATS (last access: 02/01/2024) and *hahana.soest.hawaii.edu* for HOT (last access: 02/01/2024). Note that there is a measurement gap in the HOT mesozooplankton biomass time series between 2002 and 2005.

Prior to comparing PISCES-MOG outputs with the time series observations, the latter underwent a series of post-processing steps. First, we only retained the night-time observations (18:00-7:00). Indeed, the version of PISCES used here does not represent diel vertical migration (DVM). Consequently, simulated mesozooplankton do not migrate down to the mesopelagic zone during the day, contrary to observed behavior. Thus, we posit that PISCES, operating with a 3-hourly time step and constant light forcing, primarily captures nighttime mesozooplankton vertical distribution across all time steps. This assumption is based on the hypothesis that variations in light exert minimal influence on diurnal variations in epipelagic zooplankton biomass compared to DVM. Then we

Table 4
Global Biomass of the Simulated Living Compartments and Associated Carbon Export

	Ecosystem					Biological carbon pump		
	Nanophyto. (PgC)	Diatoms (PgC)	Microzoo. (PgC)	Mesozoo. (PgC)	Total (PgC)	NPP (PgC yr^{-1})	EP100 (PgC yr^{-1})	pe-ratio (−)
PISCES-MOG	0.378	0.174	0.394	0.232	1.178	42.32	7.13	0.168
PISCES-v2	0.430	0.158	0.326	0.322	1.236	43.31	7.89	0.182
Anomaly MOG-v2 (%)	−11.9%	+9.6%	+20.8%	−27.9%	−4.7%	−2.3%	−9.6%	−7.7%
PISCES-MOG-2LS	0.366	0.168	0.427	0.232	1.194	44.80	7.02	0.157
Anomaly MOG-2LS-v2 (%)	−14.8%	+6.3%	+30.9%	−27.8%	−3.4%	+3.4%	−11.0%	−13.7%

Note. All biomass values are computed over the top 200 m. NPP100 is the Net Primary Production over the top 100 m. EP100 is the particulate organic carbon export at 100 m. pe-ratio is defined as EP100/NPP100.

converted the dry weights (mg m^{-2}) to carbon molar concentration (mmol C m^{-3}) by dividing by the maximal tow depth (200 m), multiplying by a single dry weight-to-carbon mass conversion factor of 0.35 (as per Madin et al., 2001), and dividing by the molar mass of carbon (12 g mol^{-1}). For the HOT time series, both dry weight and carbon biomass were available, allowing us to validate the use of the conversion factor at both stations (see Figure 6b). Subsequently, we averaged the time series to create monthly daytime size-resolved mesozooplankton carbon concentration climatologies at both stations.

First, to compare the observed and modeled size structure of mesozooplankton community, we computed the mean annual size spectrum at both stations by dividing the mean annual concentration of each size class by its width. Then, to analyze the size dependency of seasonality strength, we computed the relative seasonal amplitude for each mesozooplankton size class. This was done by calculating the difference between the maximum and minimum biomass of each year, normalized by the annual mean. The mean and standard deviation of the relative amplitude were then computed for each size class across the available years. Lastly, to further explore size-driven differences in temporal dynamics, we calculated a seasonal cycle for each year and each size class. To do so, we normalized each month by the mean of that year and averaged the monthly normalized values over the years, for the five size classes, at both stations.

3. Results

3.1. Simulated Ecosystem Structure and Phenology

3.1.1. Global Mesozooplankton Biomass and Community Dynamics

The total integrated annual mean biomass of all living compartments simulated by PISCES-MOG is 1.2 Pg C for the upper 200 m of the global ocean (Table 4). Primary producers account for 48% of this biomass, with the remaining 52% consisting of zooplankton, divided into unicellular heterotrophic protists (36%), juvenile metazoans (27%), and adult metazoans (37%, mesozooplankton). The contribution of each metazoan size class ranges from 3 (J_1) to 36 TgC (A_{max}), with a mean normalized biomass size spectrum (NBSS) slope of -0.80 ± 0.05, close to the theoretical size spectrum slope of -1 (Sheldon et al., 1972). The spatial distribution of the NBSS slopes indicates steeper spectra in less productive areas (e.g., −0.9 in oligotrophic gyres vs. −0.7 in the upwelling systems, see Figure S17 in Supporting Information S1), consistent with previous studies about the plankton size spectrum (see Sprules & Barth, 2016, and references within).

Spatially, simulated mesozooplankton concentration is high (>0.25 mmol C m^{-3}) in the subpolar and upwelling regions and low (<0.25 mmol C m^{-3}) in the oligotrophic gyres and at high latitudes (Figure 3a). This results in a clear zonal pattern in both hemispheres: low concentrations below 30° and above 70° latitude, and high concentrations between 30° and 60° latitude (Figure 3b). This pattern seems to be driven by primary producers, as all plankton compartments show the same zonal pattern (Figure 3b). The same zonal pattern also emerges for all adult metazoan size classes within the mesozooplankton (Figure 3c).

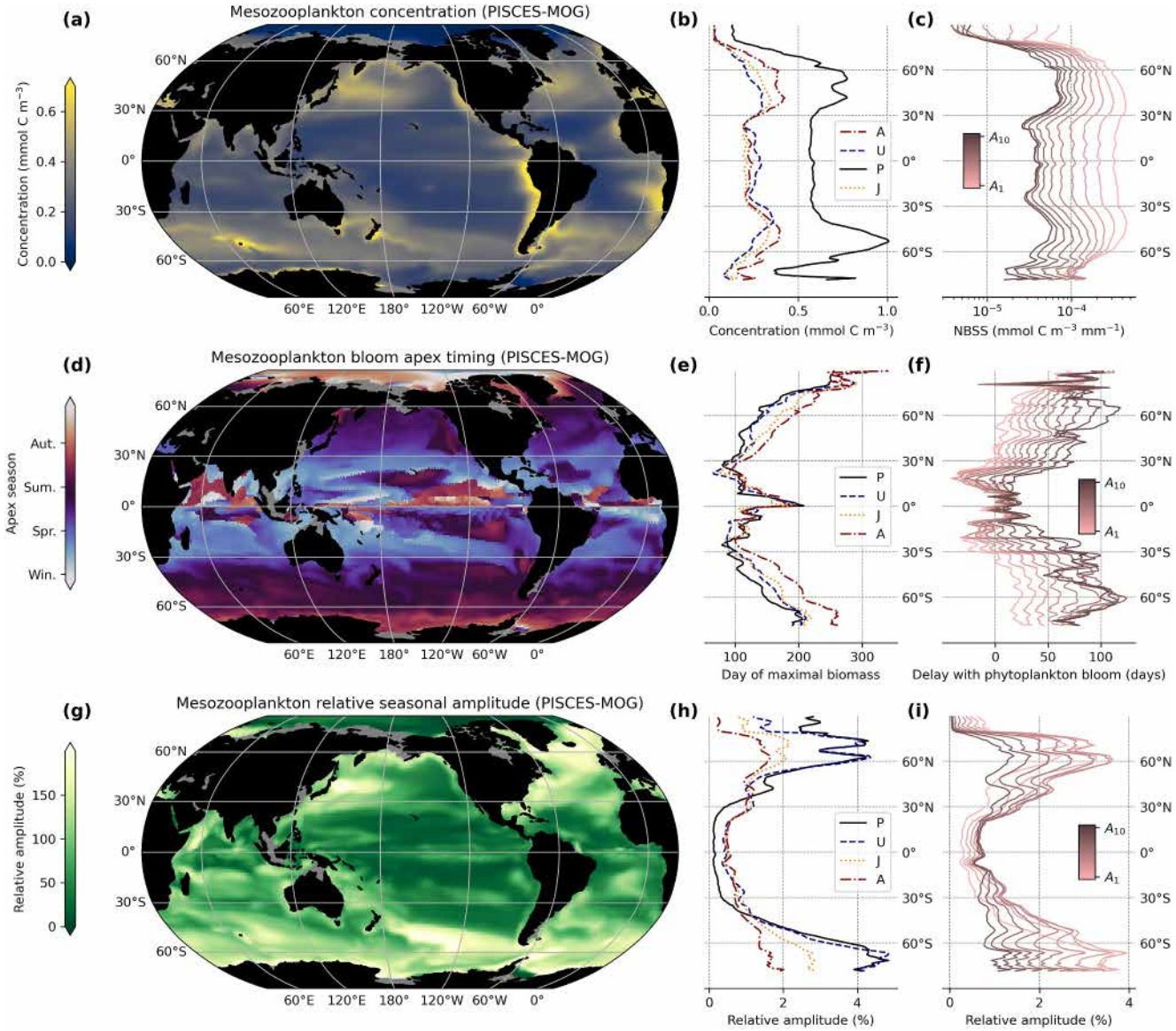

Figure 3. Global and zonally averaged epipelagic (0–200 m) plankton biomass and seasonality simulated by PISCES-MOG (a) Global average of epipelagic adult metazoans (mesozooplankton) concentration (mmol C m^{-3}). (b) Zonal mean of adult (dashed-dotted red line) and juvenile (dotted orange line) metazoans, unicellular heterotrophic protists (dashed blue line), and total phytoplankton (plain black line) concentrations (mmol C m^{-3}). (c) Mean zonal normalized biomass size spectra (NBSS, mmol C m^{-3} mm^{-1}) for the 10 adult metazoans size-classes (darker colors indicate larger size classes). (d) Global average of epipelagic mesozooplankton bloom apex (day of maximal abundance). (e) Zonal mean plankton groups bloom apexes (days, same colors as above) (f) Mean zonal delay (days) between the bloom apex of the 10 adult metazoans size classes and the bloom apexes of phytoplankton. (g) Global average of epipelagic mesozooplankton relative seasonal amplitude (%) (h) Zonal mean plankton groups relative seasonal amplitude (%, same colors as above). (i) Mean zonal relative seasonal amplitude (%) for the 10 adult metazoan size classes (darker colors indicate larger size classes).

The phenology of mesozooplankton significantly differs from that of microzooplankton and phytoplankton, both of which exhibit shorter and earlier blooms (Table 5, Figure 3e). On average, phyto- and microzooplankton bloom apexes occur 133 days after the start of the year (1st of January in the Northern Hemisphere, 1st of July in the Southern Hemisphere), whereas mesozooplankton peak 1 month later (Table 5). Bloom climax occurs 2 weeks before the bloom apex for phytoplankton, a week before the bloom apex for microzooplankton, and a month before the bloom apex for mesozooplankton (Table 5). Phytoplankton and microzooplankton show sharp but short blooms (mean duration: 64 and 70 days respectively), while mesozooplankton are characterized by longer blooms that lasts 86 days on average (Table 5). Lastly, the relative seasonal amplitude of biomass is more than 25% smaller for mesozooplankton than for microzooplankton and phytoplankton (Table 5).

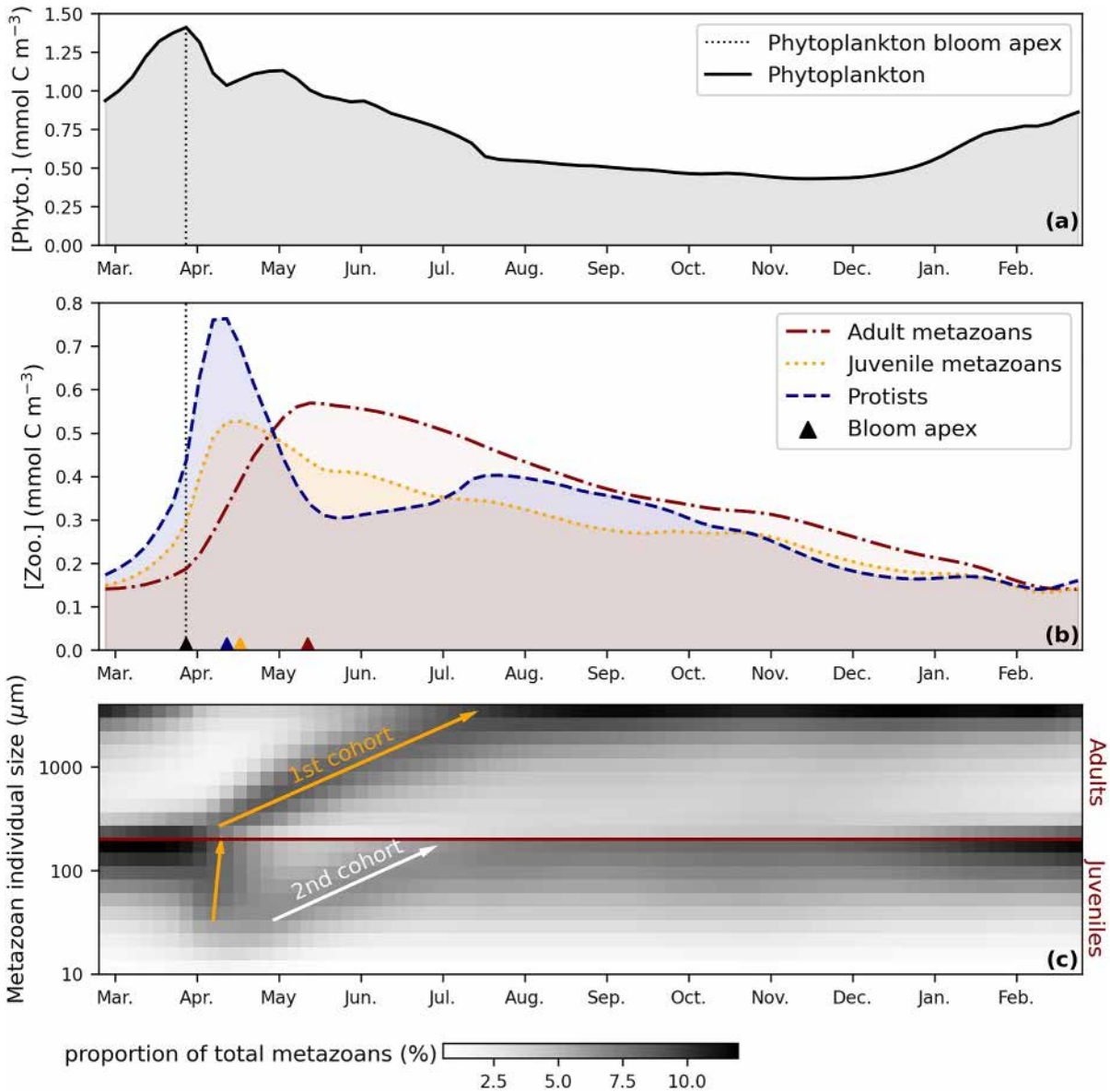

Figure 4. Seasonal dynamics of the epipelagic (0–200 m) ecosystem simulated by PISCES-MOG in the North Atlantic (46.4°N, 19.9°W) The coordinates are chosen to match the location of the North Atlantic Bloom Experiment (NABE), a pilot process study of the spring phytoplankton bloom conducted by JGOFS in 1989–1990 (Ducklow & Harris, 1993). Time evolution of (a) the phytoplankton and (b) the zooplankton concentrations (mmol C m^{-3}) over 1 year. Triangles indicate the bloom apexes of the plankton groups. (c) Change in size-class composition of metazoans over the year. The *y*-axis represents the 20 size classes ordered by increasing size. The gray levels correspond to the proportion of total metazoans (juvenile + adults) in each size classes for each time-step. Thus, for each time step, the proportions of the 20 size classes sums to 100. The arrows indicate cohorts, namely the propagation of successive waves of biomass from small to large organisms.

As latitude increases poleward, mesozooplankton phenology exhibits a later (Figure 3d) and more pronounced (Figure 3g) bloom (approximately +3 days delay and +5% in relative amplitude per degree poleward in PISCES-MOG). A similar pattern is simulated for the phytoplankton (Figures 3e and 3i), suggesting that primary producers' phenology drives the simulated zonal pattern in mesozooplankton's phenology.

3.1.2. Cohort Dynamics

Globally, all mesozooplankton size classes exhibit a zonal seasonality pattern similar to the one shown for total mesozooplankton. There is a strong latitudinal gradient in seasonality, with bloom apex (Figures 3e and 3f) and

Table 5
Global Seasonality Metrics of the Simulated Living Compartments

		Phytoplankton	Microzoo.	Mesozoo.
Relative seasonal amplitude (%)	PISCES-MOG	121%	107%	93%
	PISCES-v2	115%	132%	111%
	Anomaly MOG-v2	6%	−25%	−18%
Bloom apex (day)	PISCES-MOG	133	133	159
	PISCES-v2	133	129	161
	Anomaly MOG-v2	0	4	−2
Bloom climax (day)	PISCES-MOG	117	124	130
	PISCES-v2	116	124	133
	Anomaly MOG-v2	1	0	−3
Bloom duration (days)	PISCES-MOG	64	70	86
	PISCES-v2	62	60	80
	Anomaly MOG-v2	2	10	6

Note. Variables are defined in Section 2.2.3 of the methods. All values are computed over the top 200 m. Global averages are weighted by the corresponding plankton biomass distribution simulated in PISCES-MOG (the same weights are applied to PISCES-v2 and PISCES-MOG for consistency in the anomaly computation. Note that applying weights from PISCES-v2 would result in similar averages).

bloom climax (Figures S6d, S6e, S6f in Supporting Information S1) occurring later as latitude increases poleward. The relative seasonal amplitude of mesozooplankton biomass increases poleward (Figure 3h).

Moreover, PISCES-MOG simulations reveal a size class dependency of mesozooplankton dynamics: larger size classes peak later than smaller ones, with the largest size classes peaking up to 3 months later than the smallest one (Figure 3f). This trend aligns with the temporal trend of other metrics: larger size classes have a later bloom climax (Figure S6f in Supporting Information S1) and a longer bloom duration (Figure S6c in Supporting Information S1), along with a lower seasonal amplitude (Figure 3j). Note that a similar size class dependency is simulated for juvenile metazoans dynamics (Figures S7 and S8 in Supporting Information S1). These size-dependent variations in bloom metrics indicate a cohort dynamics, a phenomenon in which biomass spreads across the size spectrum due to synchronous growth and/or reproduction. This behavior is extensively described in the chemostat model of plankton dynamics by Clerc et al. (2021). The biogeochemical conditions driving metazoan cohort dynamics in Clerc et al. (2021) aim to replicate those in the North Atlantic, where zooplankton phenology is influenced by a strong phytoplankton spring bloom. To further characterize this pattern in PISCES-MOG, we analyze the temporal dynamics of plankton at a grid point representative of the well-studied North Atlantic bloom system: NABE (46.4°N, 19.9°W).

As expected, PISCES-MOG simulates a phytoplankton bloom in early spring at NABE, reaching its peak in early April (Figure 4a). This triggers a zooplankton bloom: microzooplankton (heterotrophic protists and juvenile metazoans) peak around 15 days later, while mesozooplankton peak 45 days later (Figure 4b). The temporal evolution of the metazoan composition shows a wave signal driven by a cohort dynamic, as demonstrated in Clerc et al. (2021). Before the phytoplankton spring bloom, biomass is distributed similarly in both juvenile and adult metazoan groups; larger organisms are more abundant than smaller ones (Figure 4c). The bloom triggers an increase in food availability, leading to population growth. Smaller organisms, that are characterized by higher maximal grazing rates, experience a faster increase in concentration than larger organisms, resulting in a higher proportion of biomass accumulating in smaller size classes at the beginning of April (Figure 4c). Ontogenetic growth results in the transfer of this biomass to the larger juvenile size classes (orange arrow) and then to adults (orange arrows in Figure 4c). This characterizes the formation of a first cohort. Reproduction of the adults from this first cohort results in a second cohort, for which the signal is lost in the adult size classes (white arrow, Figure 4c). Note that a similar cohort pattern also emerges under the oligotrophic conditions prevalent at BATS (Figure S9 in Supporting Information S1) and at HOT even though the signal is weaker there (Figure S10 in Supporting Information S1).

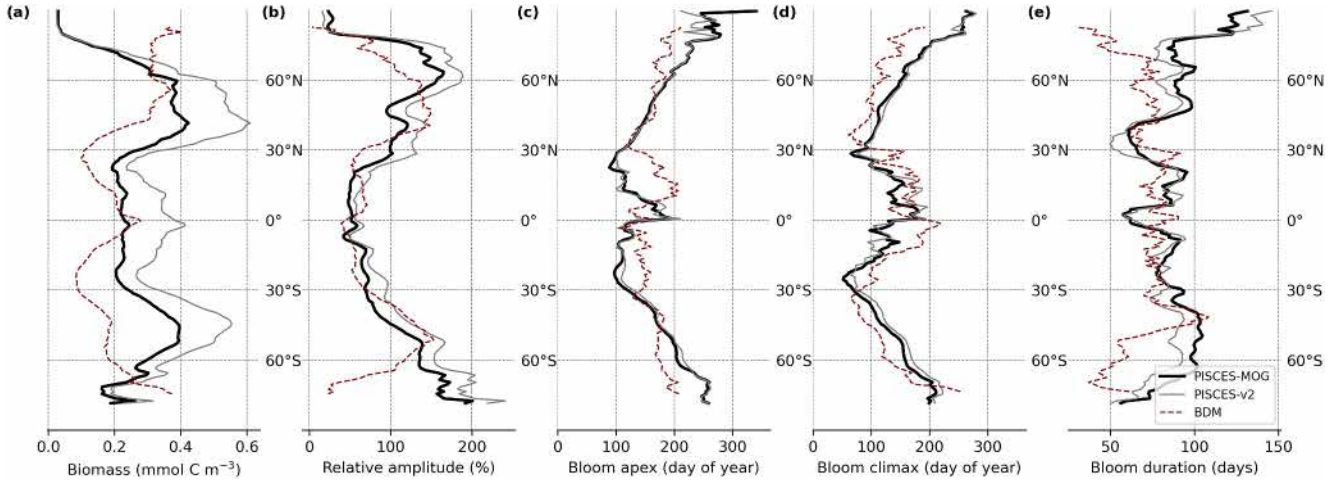

Figure 5. Model-data comparison of the mesozooplankton biomass and its seasonality. For each of the five evaluated metrics, we compare the zonal mean of the metric computed on the mesozooplankton distribution simulated by PISCES-v2 (gray line), PISCES-MOG (black line) and interpolated from observation (BDMs-MAREDAT, dotted red line). The five metrics evaluated are (a) biomass (mmol C m^{-3}), (b) relative seasonal amplitude (%), (c) bloom apex (day of the year), (d) bloom climax (day of the year) and (e) bloom duration (days). The metrics are defined is the methods Section 2.2.3.

3.2. Comparison of PISCES-MOG Outputs to Observations

Next, we focus on the evaluation of the key new component of the PISCES-MOG model (absent in PISCES-v2): the size-structured mesozooplankton compartment. In the supplementary material, we present an evaluation of nitrate and chlorophyll distributions (Figure S11 in Supporting Information S1) and chlorophyll dynamics (Figure S12 in Supporting Information S1). For these tracers, note that the performance of PISCES-MOG is similar to that of PISCES-v2 (Aumont et al., 2015).

3.2.1. Evaluation of Simulated Total Mesozooplankton Biomass and Seasonality Against Observation-Based Products

The annual mean distribution of total mesozooplankton biomass as well as the distribution of the four seasonality metrics defined in Section 2.2.3 are compared to the BDMs-based climatology. Overall, the quantitative statistical evaluation shows that PISCES-MOG successfully simulates mesozooplankton biomass and phenology at the global scale (Table 3) and zonally (Figure 5).

We find that both biomass distributions align in their overall order of magnitude (total epipelagic biomass: 137 TgC in the BDMs-based climatologies vs. 232 TgC in the PISCES-MOG outputs). PISCES-MOG and BDMs-based global mesozooplankton biomasses are significantly correlated (Pearson $r = 0.4$, p-value $< 10^{-15}$, Table 3 and Figure S13 in Supporting Information S1). In productive systems, such as upwelling areas, and less productive systems, such as oligotrophic gyres, both observed and modeled climatologies consistently depict higher and lower biomass levels, respectively (Figure 5a, Figure S13 in Supporting Information S1). Spatial variability is also consistent between the model-based outputs and observations (Table 3).

The seasonality metrics and their standard deviations are consistent between PISCES-MOG outputs and observation-based fields on a global scale (Table 3, Figure S13 in Supporting Information S1), with biases lower than 20%. However, PISCES-MOG tends to simulate earlier and longer mesozooplankton blooms than computed from the BDMs-based climatology (Table 3, Figures 5c and 5d). While the correlation coefficients for bloom climax and bloom apex between the model-based and the BDMs-based outputs are r^2; = 0.23 and 0.32 (Table 3), the spatial distribution is consistent between the two estimates. Both outputs indicate a later bloom as latitude increases poleward, at a rate of approximately +3 days per degree in PISCES-MOG and +2 days per degree in the BDMs-based climatology (Figures 5c and 5d). In the tropical band (i.e., between 30°S and 30°N), where the seasonal signal is low (<80%, Figure 5b), the bloom apex and bloom climax distribution are patchy in both the model-based and the BDMs-based fields (Figures 3d and 5c, 5d, S6d, S14d, S15d in Supporting Information S1), as intra-annual variations are not driven by seasonality in these regions at the first order. In contrast, bloom duration is poorly

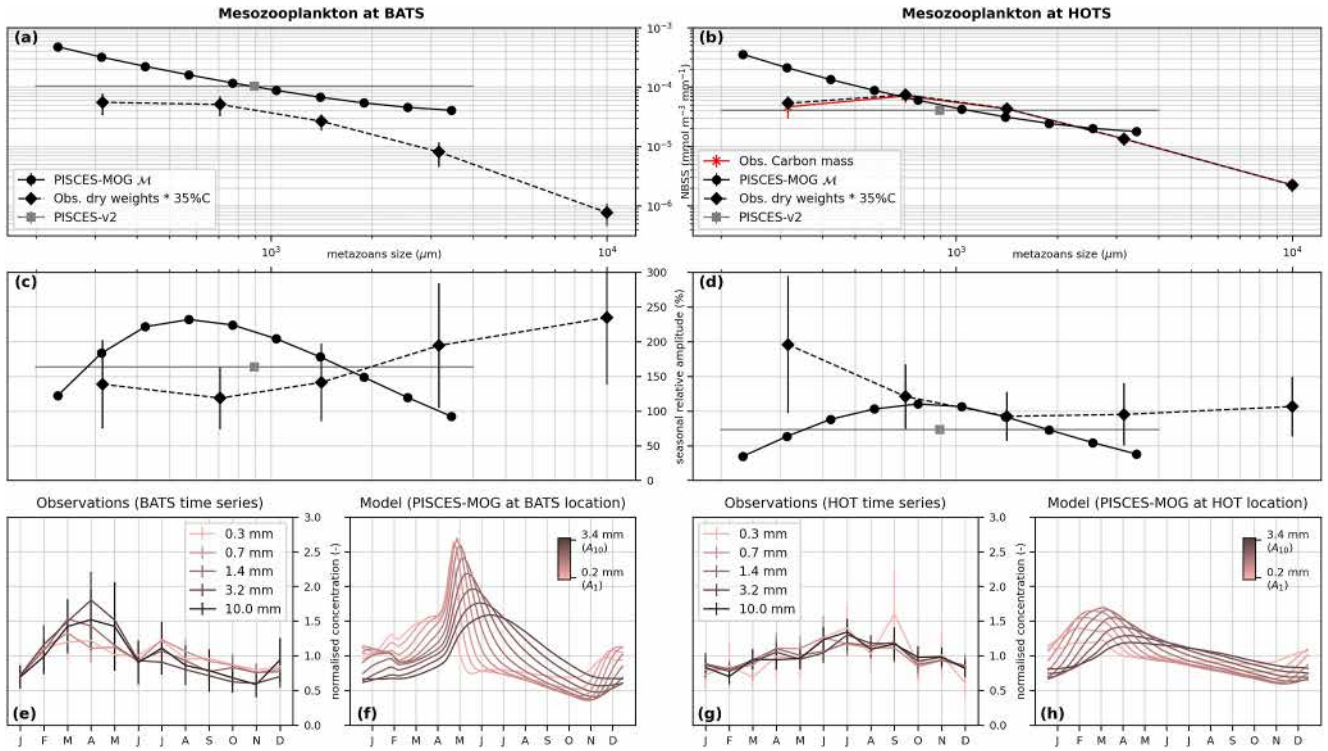

Figure 6. Model-data comparison of mesozooplankton biomass and seasonality at BATS (32.1°N 64.0°W, left panels) and HOT (25.1°N 158.0°W, right panels). (a, b) (respectively c, d) Normalized biomass size spectra (NBSS, in mmol C m^{-3} mm^{-1}) (respectively relative seasonal amplitude, in % of yearly average biomass). The time series of the 10 adult metazoan size classes simulated by PISCES-MOG are represented by black lines with round dots. The squared gray dot refers to the PISCES-v2 total mesozooplankton time series. Black dotted lines with lozenge dots represent observed mesozooplankton dry weight time series converted to carbon concentrations for the five size classes (see Section 2.3.2). Note that for the larger observed size class, the mean individual size is arbitrarily set to 10 mm since the upper size limit is unknown, but is not considered when computing size spectrum slopes. For (b), the red line indicates the size spectrum computed from carbon content values, available only for the HOT time series, illustrating the consistency of our dry-weight to carbon conversion. Error bars in observations represent inter-annual variability. (e–h) Normalized seasonal cycle for each observed and modeled mesozooplankton biomass time-series by size class. Normalization is based on yearly average biomass, with error bars indicating inter-annual variability of the normalized seasonal cycle. The color represents the mean size of the class (light pink for smaller sizes to dark brown for larger size classes). Note that error bars are absent for model outputs in all panels (a–h) since PISCES is forced with a 1-year climatology.

correlated between the model-based and the BDMs-based fields ($r = 0.04$, Table 3, Figure 5e). No clear large-scale pattern emerges from the model and observation for this metric, as bloom duration seems to be uniformly patchy across the global ocean (Figures S6a and S15a in Supporting Information S1). Relative biomass amplitudes are spatially consistent between the model-based and the BDMs-based fields ($r = 0.52$, Table 3, Figure 5b), with the dominating pattern being an increase in relative amplitude toward the poles (Figures 3g and S16a in Supporting Information S1). Therefore, PISCES-MOG consistently simulates large-scale mesozooplankton spatial and intra-annual variability, even though bloom duration is poorly constrained due to its patchiness.

3.2.2. Evaluation of Modeled Mesozooplankton Size Structure Against Time-Series Data

To our knowledge, no global monthly climatologies of mesozooplankton size structure based on field observation are currently available. Thus, our evaluation of mesozooplankton size structure is limited to the observations from the two time series stations, BATS and HOT. Note that observed mesozooplankton time-series were not available at NABE, where we described an emergent metazoan cohort dynamics in PISCES-MOG (Section 3.2.2). However, PISCES-MOG simulates a cohort pattern at HOT and BATS that is similar to the one simulated for NABE (see Figures S9 and S10 in Supporting Information S1).

We divided the evaluation of the seasonal patterns in mesozooplankton size structure at the HOT and BATS stations into three parts: (a) the comparison of the size spectra aims to evaluate the size structure of the mean annual biomass (Figures 6a and 6b), (b) the comparison of relative seasonal amplitudes investigates the size-

dependent variations in seasonal biomass (Figures 6c and 6d), and (c) the comparison of normalized seasonal cycles evaluates the relationship between size and the temporal structure of seasonality (Figures 6e and 6f).

Consistent with Sheldon's theoretical hypothesis (Sheldon et al., 1972), the slope of the spectrum is not significantly different from −1 (p-values > 0.05) for the model-based outputs and the observations at both stations (modeled respectively observed, size spectrum slopes are −0.92 respectively −0.84 at BATS, −1.12 respectively −0.61 at HOT, Figures 6a and 6b). Note that, for the time series observations, the size spectrum's normalized biomass (NBSS) value (Figures 6a and 6b) is likely underestimated for the small size class due to the detection limit corresponding to the net mesh size (202 μm). This explains the misalignment of the smaller size class point in both field-based size spectra. The model overestimates biomass at BATS by a factor of 4 (Figure 6a) but performs well at HOT (mean model over obs. ratio <1.5, Figure 6b). As a result, a simple parameterization of mesozooplankton allows the introduction and evaluation of a consistent size-spectrum structure in PISCES-MOG, which was absent in PISCES-v2.

The relative seasonal amplitude of mesozooplankton biomass is consistent between the model and observations at both stations, with overlapping ranges, although the mean amplitude is consistently lower at HOT compared to BATS (Figures 6c and 6d). Although PISCES-MOG exhibits a clear bell-shaped size structure in relative seasonal amplitude, with lower seasonal amplitudes for the smallest and largest size classes, the inter-annual variability of the observations is too high to delineate differences in seasonality across size classes (Figures 6c and 6d).

The comparison of the observed and modeled mesozooplankton temporal dynamics is limited by the inter-annual variability in the observations. PISCES-MOG predicts a bloom that occurs between one and 2 months later than the ones reported at BATS (April-July vs. March-May, Figure 6e). It also predicts a marked shift in the timing of maximum biomass with increasing size that is consistent with a cohort process (Figure 6e, see Section 3.1.2). A similar pattern appears in the observations, but the high inter-annual variability makes it difficult to discern a significant pattern. At HOT also, a cohort pattern is observed in the model, with bloom peaks occurring between February and April (Figure 6f). However, analyzing the seasonality in observations at HOT is even more challenging than at BATS due to the high inter-annual variability and the low seasonal variability (Figure 6g).

In summary, while the evaluation of mesozooplankton size structure and seasonality showed that PISCES-MOG performs reasonably well, evaluating the size structure of the seasonal signal remains challenging. Yet, we note that both BATS and HOT are stations located in oligotrophic gyres, where both productivity and seasonality are known to be low all year long. This could explain why observations have a low seasonal signal versus inter-annual variability ratio.

3.3. Biogeochemical Impacts of the Representation of Mesozooplankton Ontogenetic Growth and Reproduction

In order to quantify the impacts of mesozooplankton ontogenetic growth and reproduction, in this section we compare PISCES-MOG and PISCES-v2. We first compare the ecosystem structure and phenology between the two models, and then show how these differences between models induce different carbon fluxes.

3.3.1. Impacts on the Ecosystem Structure

The simulated total living epipelagic biomass shows minor variation (<5% difference) between PISCES-v2 and PISCES-MOG, with respective estimates of 1.18 and 1.24 GtC over the top 200 m (Table 4). The inclusion of mesozooplankton ontogenetic growth in PISCES-MOG results in juvenile metazoans biomass redistribution from the mesozooplankton biomass pool to the microzooplankton pool. Consequently, total mesozooplankton biomass is 28% lower and total microzooplankton 21% higher in PISCES-MOG compared to PISCES-v2 (Table 4). Thus, while total zooplankton (i.e., micro- and mesozooplankton together) biomass is only slightly affected by the inclusion of a more complex mesozooplankton representation (−3.4% in PISCES-MOG compared to PISCES-v2, Table 4), the repartition within size-based compartments is different (i.e., mesozooplankton represents 50% of total zooplankton in PISCES-v2, 38% in PISCES-MOG, Table 4).

These changes in biomass distribution impact the overall ecosystem structure significantly. As zooplankton exert a top-down control on primary producers through grazing, changes in zooplankton composition modify predation pressure and thus impact phytoplankton composition. Indeed, PISCES includes an explicit representation of two phytoplankton groups: nanophytoplankton that are mainly grazed by microzooplankton, and diatoms that are

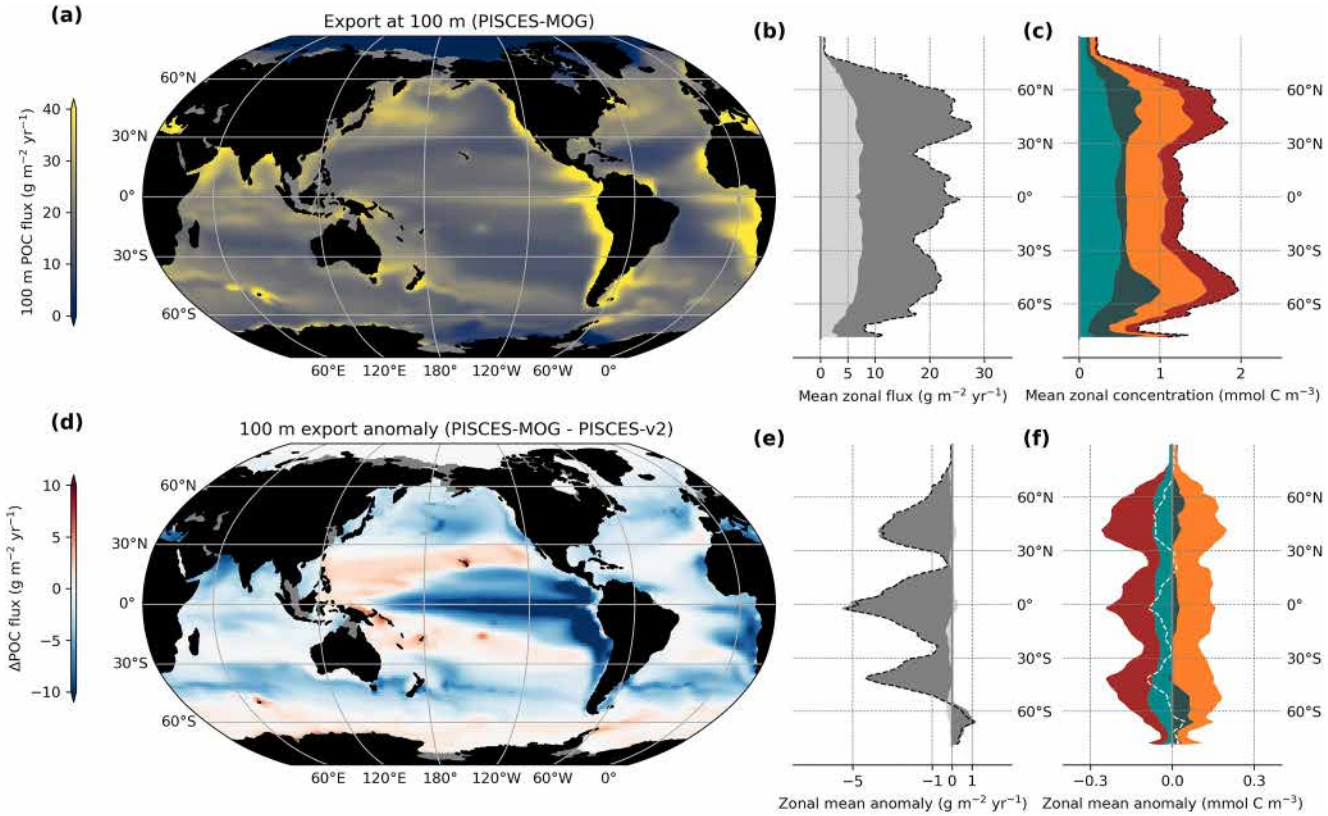

Figure 7. Global particulate organic carbon (POC) flux estimates, particle composition and biological drivers in PISCES-MOG and PISCES-v2. (a) Global distribution of POC export at 100 m (gC m^{-2} yr^{-1}) simulated in PISCES-MOG and (d) relative anomaly compared to PISCES-v2 (b) Zonal mean POC export at 100 m (gC m^{-2} yr^{-1}) and (e) relative anomaly compared to PISCES-v2. The dashed line shows the total POC. The fill colors show the contribution of the different components of the POC: small particles in light gray, large particles in dark gray. (c) Zonal mean community composition (mmol C m^{-3}) in PISCES-MOG and (f) relative anomaly compared to PISCES-v2. The dashed line shows the total simulated living concentration. The fill colors show the different groups of organisms: from left to right in panel (c), nanophytoplankton in blue, diatoms in dark blue, microzooplankton in orange and mesozooplankton in dark red.

mainly grazed by mesozooplankton. As a consequence of this top-down control by zooplankton, a decrease of 12% of nanophytoplankton biomass is simulated in PISCES-MOG compared to PISCES-v2 due to an increase in predation pressure mediated by an increase in microzooplankton (Table 4). Similarly, an increase of 10% in diatom biomass is simulated in PISCES-MOG due to a relaxation of predation pressure by mesozooplankton (Table 4). These effects on the epipelagic ecosystem structure are qualitatively similar across latitudes (Figure 7f).

3.3.2. Impacts on Plankton Phenology

We evaluate the differences in seasonal patterns between PISCES-v2 and PISCES-MOG for latitudes beyond 20° based on 5-day-average time series (Table 5).

Differences in seasonality are small between PISCES-MOG in PISCES-v2 (Table 5). The timing of the bloom apex and bloom climax varies by a few days in the two models for micro- and mesozooplankton (Table 5, Figure 5). The impacts on phytoplankton phenology are even smaller (i.e., <2 days). However, annual absolute amplitudes are affected consistently with the change in absolute biomass: mesozooplankton seasonal amplitude is reduced by 39%, while it is increased by 6% for microzooplankton (Table 5). More interestingly, while absolute amplitudes show opposite patterns for meso- and microzooplankton, relative amplitudes are reduced by more than a quarter in both groups (Table 5). This can be explained by the subdivision into classes that have differential seasonality (cohort pattern, see Section 3.1.2), which flattens the seasonal signal of the whole group. This is confirmed by the bloom duration, which increases by 17% for microzooplankton and 8% for mesozooplankton in PISCES-MOG compared to PISCES-v2 (Table 5).

Therefore, while the introduction of ontogenetic growth in PISCES-MOG modifies the ecosystem structure and the seasonal amplitude of total mesozooplankton significantly, its impact on total mesozooplankton biomass seasonality remains limited, even if there are large intra-compartment variations in biomass seasonality due to cohort dynamics (see Section 3.1).

3.3.3. Impacts on the Carbon Cycle

The efficiency of carbon transfer to the deeper layers strongly relies on the sinking speed of particles which is highly size-dependent (Cael et al., 2021). In both PISCES versions, POC is split into two groups: small organic carbon particles, which sink at a speed of 2 m d^{-1}, and large particles, which sink at a speed of 50 m d^{-1}. Consequently, for an identical remineralization rate, carbon contained in large particles will be exported 25 times more efficiently than carbon contained in small POC. Moreover, while mesozooplankton particle production is mainly directed toward large POC, microzooplankton-produced particles are considered small particles. As a direct consequence of simulated changes in zooplankton composition in PISCES-MOG compared to PISCES-v2, POC flux at 100 m is reduced by 10% in PISCES-MOG (Figures 7a and 7d). This change is mainly driven by the decrease in the flux associated to large particles (responsible of 97% of the total flux decrease, Figures 7b and 7e) caused by the decrease in mesozooplankton biomass (Figures 7c and 7f). The net primary production being similar in PISCES-v2 (43.3 PgC yr^{-1}) and PISCES-MOG (42.3 PgC yr^{-1}), this reduced export in PISCES-MOG is associated to an 8% lower pe-ratio.

Spatially, the changes in export are driven by changes in mesozooplankton biomass in the productive regions, since maxima in mesozooplankton decline at around 40° latitude and at the Equator (Figure 7f) correlate with peaks in large particles' decline at the same latitudes (Figure 7e). As a result, the equatorial upwelling and the sub-polar productive zones contribute the most to the decline in 100 m export when accounting for mesozooplankton reproduction and ontogenetic growth (Figure 7d).

While the introduction of mesozooplankton ontogenetic growth and reproduction into PISCES significantly reduces the mean annual export of particulate organic carbon (POC) at 100 m depth in the ocean, its impact on the seasonality of this flux is limited. Changes of less than 5 days in the global average for particles bloom apexes and climaxes, not presented here, indicate this limited effect. This expected behavior results from the limited influence of mesozooplankton ontogenetic growth and reproduction on the seasonal timing of various organism groups (see Section 3.3.2).

3.3.4. Relative Contributions: The Relative Role of Reproduction and Ontogenetic Growth Versus That of the Representation of Size

The addition of explicit reproduction and ontogenetic growth versus the addition of a full size spectrum could have differential effects on the behavior of PISCES-MOG. To disentangle their relative importance, we compare PISCES-MOG versus PISCES-v2 anomalies to PISCES-MOG-2LS versus PISCES-v2 anomalies (Table 4, models defined in Section 2.2.2). We identified three possible scenarios: (a) If PISCES-MOG anomalies are similar to PISCES-MOG-2LS anomalies, the size spectrum representation has little impact on the behavior of PISCES-MOG. In this case, the simulated differences between PISCES-MOG and PISCES-v2 are driven by the introduction of ontogenetic growth and reproduction. (b) If there is a lower absolute anomalies in PISCES-MOG-2LS compared to PISCES-MOG, the impact of reproduction and ontogenetic growth on the model behavior is amplified when representing the size spectrum. (c) If there is a higher absolute anomaly in PISCES-MOG-2LS compared to PISCES-MOG, the size spectrum representation actually dampens the effect of representing ontogenetic growth and reproduction.

Based on these scenarios, we disentangle the relative effect of reproduction and ontogenetic growth versus that of the representation of size. PISCES-MOG-2LS and PISCES-MOG show consistent biomass anomaly signs across all plankton groups (Table 4). However, micro- and nanophytoplankton anomalies are 30%–50% higher, while diatom anomalies are 30% lower in PISCES-MOG-2LS compared to PISCES-MOG (Table 4). Consequently, diatoms and mesozooplankton are less abundant in PISCES-MOG-2LS, leading to a 20% higher absolute export flux anomaly (Table 4). In PISCES-MOG-2LS, NPP shows an opposite anomaly compared to PISCES-MOG, resulting in a doubling of the PE-ratio anomaly. Thus, the effect of metazoan ontogenetic growth and reproduction representation on the intensity and efficiency of the BCP is dampened by the representation of a size spectrum. Spatially, both models show similar anomaly distributions for most plankton groups, except for diatoms in the

Southern Ocean (Figure S1 in Supporting Information S1). Despite this difference, the resulting export flux anomaly distribution is similar in both models for most ocean regions (Figure S2 in Supporting Information S1). Thus, in PISCES-MOG, metazoan reproduction and ontogenetic growth representation primarily drive differences with PISCES-v2 behavior.

4. Discussion

4.1. Changes in Plankton Biomasses and Carbon Export Estimates

Incorporating a detailed representation of mesozooplankton ontogenetic growth and reproduction into a biogeochemical component of an earth system model did not alter the realism of PISCES biogeochemical global properties. Indeed, in PISCES-MOG, spatial patterns are primarily related to the global gradient in primary productivity. This results in high biomasses in high-latitude regions and low biomasses in oligotrophic gyres, consistent with observations (Hatton et al., 2021). Net primary production (NPP, 42 PgC yr^{-1}) and carbon export estimates at 100 m (EP100, 7.1 PgC yr^{-1}), fall within the range of the literature: 5.8–9.1 PgC yr^{l} for EP100 (Clements et al., 2023; DeVries & Weber, 2017; Siegel et al., 2014) and 35–77 PgC yr^{-1} for NPP (Field et al., 1998; Westberry et al., 2023).

However, incorporating mesozooplankton ontogenetic growth and reproduction led to significant changes in annual biomass distribution within plankton compartments relative to the standard version of the model. As anticipated in Clerc et al. (2021), zooplankton biomass was partly redistributed toward microzooplankton because adult metazoans allocate a portion of their energy toward reproduction. This behavior enhances the realism of PISCES. Indeed, *Copepoda*, recognized as the most abundant mesozooplankton group (Drago et al., 2022; Moriarty & O'Brien, 2013), can represent a significant portion of microzooplankton at their nauplii stages (up to 30%; Quevedo & Anadón, 2000; Safi et al., 2007). In addition, PISCES-MOG simulated mesozooplankton biomass distributions are closer to our present BDMs-based biomass estimates compared to the distributions simulated by PISCES-v2 (Figure 6), suggesting that PISCES-MOG simulations are closer to field observations. Thus, PISCES-MOG simulates zooplankton more accurately than PISCES-v2, which may lead to increased realism in biogeochemical fluxes.

As a consequence of the changes in zooplankton structure, the particle size distribution shifted toward smaller particles (Section 3.3.3). Consequently, the export at 100 m was 10% lower in PISCES-MOG compared to PISCES-v2. This finding suggests that including ontogeny would result in lower zooplankton-driven carbon export in many biogeochemical components of Earth System Models, as these often represent mesozooplankton as one class of large organisms producing fast sinking particles (Kearney et al., 2021). However, adding a more complex representation of the mesozooplankton would increase the computational cost by a factor of 2 or even more in fully coupled Earth System Models experiments, where physical and biogeochemical processes interact in both ways (such as in the Climate Model Intercomparison Project exercises, Eyring et al., 2016; Taylor et al., 2012). In parallel, the sensitivity experiment based on PISCES-MOG-2LS, where the representation of metazoan zooplankton is limited to two size classes instead of 20 (one juvenile compartment and one adult organism compartment, Section 2.2.2) resulted in similar changes in biomass distribution and changes in carbon export compared to the changes observed when comparing PISCES-MOG to PISCES-v2 (Section 3.3.4). Therefore, mesozooplankton ontogenetic growth and reproduction could be included in biogeochemical models without inducing a significant increase in computational cost by simply including a juvenile metazoan compartment in the microzooplankton. This simple addition would likely suffice to influence the dynamics of carbon export in a manner similar to adding a complete representation of mesozooplankton ontogenetic growth and reproduction.

4.2. Cohort-Driven Impacts on Plankton and Carbon Cycling

To our knowledge, this is the first study to specifically diagnose potential shifts in zooplankton phenology induced by incorporating of full size spectrum representation in a global biogeochemical model. By representing metazoan size classes the same way as in the 0D chemostat model of Clerc et al. (2021), we successfully introduced cohort dynamics for metazoans in PISCES-MOG. Indeed, the seasonal behavior of each size class showed a globally consistent pattern: larger metazoans peak later and their blooms last longer. These cohort dynamics is consistent with patterns previously evidenced in the field (Mackas et al., 2012) and in models (Maury

et al., 2007; McCauley & Murdoch, 1987; Persson et al., 1998; Pope et al., 1994; Zhou et al., 2010). They emerge because juveniles display a competitive advantage over adults right after a phytoplankton bloom thanks to their higher mass-specific ingestion rates (De Roos et al., 2008; De Roos & Persson, 2003; Persson & de Roos, 2013; Persson et al., 1998).

We expected cohort dynamics to induce a temporal delay in the peak of mesozooplankton biomass within the year, compared to the peak simulated by a model without cohorts (Clerc et al., 2021). Surprisingly, the inclusion of mesozooplankton ontogenetic growth and reproduction did not significantly modify the temporal dynamics of mesozooplankton biomass in the 3-D implementation of the Clerc et al. (2021) model (Table 5). To explain this, we argue that the metazoan population size structure right before the phytoplankton bloom (i.e., pre-bloom conditions) plays a determining role in the simulated temporal dynamics. In Clerc et al. (2021) the pre-bloom metazoan population consisted of adult stages only. Due to the lower growth rate of adults compared to other smaller metazoan size classes, this population structure resulted in a slow formation of the first cohort, significantly contributing to the simulated delay in the peak of mesozooplankton compared to the model without ontogenic growth and reproduction. In PISCES-MOG, pre-bloom metazoan size classes are more evenly distributed among juveniles and adults (Figure 4). This structure led to a faster cohort formation than in Clerc et al. (2021) and eliminated the delay in the peak of mesozooplankton biomass between PISCES-MOG and PISCES-v2 (Table 5).

Including mesozooplankton ontogenetic growth also had limited impact on the seasonality of carbon export (Section 3.3.3). However, we argue that the effects on carbon flux seasonality are underestimated because the particles produced by any mesozooplankton size class are all directed to the same particle pool. We hypothesize that representing a particle size spectrum in PISCES-MOG would delay the annual peak in carbon export, because particles produced by each mesozooplankton size class would be allocated to distinct particle size classes. Small metazoans that peak earlier (Section 3.1.2), would produce small particles that sink slowly (Cael et al., 2021). Large metazoans that peak later (Section 3.1.2), would produce large particles that sink fast. Thus, by introducing a particle size spectrum, the particle export efficiency would increase over time after the phytoplankton bloom, and consequently POC flux export peak would be delayed. Using a numerical model representing a particle size spectrum, Serra-Pompei et al. (2022) showed that size-spectrum slope and trophic levels of copepods (that can be linked to the size) are important drivers of carbon export and carbon export efficiency (pe-ratio), respectively. This supports our hypothesis that including particles size spectrum in PISCES-MOG would result in changes in POC flux seasonality when accounting for mesozooplankton ontogenetic growth.

4.3. Evaluating Mesozooplankton Phenology and Size Structure in Marine Biogeochemical Models

We emphasize that new observation-based BDMs provide valuable insights into the seasonal patterns of global zooplankton biomass, as they unlock spatial and temporal scales that are not covered by the previous observations. Observations-based biomass products from MAREDAT (Moriarty & O'Brien, 2013) or subset, such as COPEPOD (O'Brien, 2005), are often used to evaluate the predictions made by marine ecosystem models for various plankton functional types in point-by-point comparisons (Aumont et al., 2015; Clerc, Bopp, et al., 2023; Le Quéré et al., 2005; Stock et al., 2014). This evaluation is limited by the restricted spatiotemporal scales covered by these observational data. Here, we benefit from novel approaches established to develop distribution models based on continuous abundance and derived biomass observations (Drago et al., 2022; Knecht et al., 2023; Waldock et al., 2022). Indeed, for the first time to our knowledge, we were able to evaluate the skill of a global biogeochemical model in predicting the phenology and the seasonal production patterns of zooplankton against an observation-based product. BDMs can thus successfully extract and extrapolate biomass patterns in space and time, and substantially reduce the noise levels in biological data, enabling their comparison with biogeochemical model outputs. Our work represents a key step toward improving the assessment of zooplankton functional groups in Earth System Models, as we anticipate that further versions of such data-driven extrapolated biomass distribution products will emerge for multiple plankton functional types (PFT), like those developed for crustaceans and radiozoa based on imaging data (Drago et al., 2022) and those for pteropods and foraminifers based on traditional net data (Knecht et al., 2023).

Unlike previous versions of PISCES, a new feature requiring evaluation against field observations is the mesozooplankton size spectrum. However, we identified only two open-ocean time series that provided sufficient information to assess both the zooplankton size spectrum and its seasonality. While modeled and observed zooplankton size spectra exhibited similarities, both time series displayed significant inter-annual variation in seasonality, precluding the identification of size-dependent seasonal patterns. In this context, zooplankton community monitoring using imaging methodology (e.g., Lombard et al., 2019) paired with machine learning and BDM techniques are promising tools to (a) increase the number of observations, and (b) extrapolate between measurements at a global scale. Specifically, Under Vision Profiler 6 (UVP6) images are expected to significantly contribute to constraining zooplankton size spectrum dynamics globally (Picheral et al., 2022). Indeed, particle size distribution can be extracted from the images with novel machine learning tools that enable the quantification and monitoring of zooplankton functional traits from a wealth of in situ imaging observations (Irisson et al., 2022; Orenstein et al., 2022). Thus, the integration of imaging-derived in situ zooplankton size observations with machine learning and BDM techniques would enable the evaluation of size-structured zooplankton global dynamics simulated by our model.

4.4. Model Caveats

The extraordinary diversity of zooplankton life histories leads to complex responses to environmental conditions and seasonal successions between different organisms (Kenitz et al., 2017; Romagnan et al., 2015). In contrast, the way we incorporated mesozooplankton ontogenetic growth and reproduction remains simplified due to computational constraints and does not account for all sources of intra- and interspecific variability within the mesozooplankton life histories (Mauchline, 1998). First, we assumed that all adult metazoans can reproduce. However, large species can reach a size considered as adult in PISCES-MOG before reaching sexual maturity (Hartvig et al., 2011). A consequence of that assumption is that the biomass and pool of reproductory organisms is overestimated, leading to a likely overestimate of simulated reproduction rates. A more realistic representation of reproduction would necessitate multiple size spectra organized based on maximum size (Hartvig et al., 2011) or to make coarse assumptions about the maximum reproduction rates (Baird & Suthers, 2007), and this would likely reduce the differences in annual biomass and POC fluxes between PISCES-MOG and PISCES-v2.

Second, zooplankton are assumed to be "income breeders" (Sainmont et al., 2014) in PISCES-MOG, meaning that a portion of the grazing flux is instantaneously allocated to reproduction (Section 2.2.2). However, some organisms adopt an alternative reproduction strategy called "capital breeding" (Varpe et al., 2009), according to which an individual may allocate energy to reserves which are used later in the year for reproduction. For example, certain copepod species undergo one or more diapause stages throughout their life cycle to overcome unfavorable conditions (Baumgartner & Tarrant, 2017; Hirche, 1996). This pause in biological development can occur at various life stages, including eggs, embryos, juveniles, and adults and lead to synchronous metazoan life cycles (Brun et al., 2016). Consequently, representing this additional process in PISCES-MOG could affect the pre-bloom metazoan population size structure by delaying the peak of mesozooplankton biomass between PISCES-MOG and PISCES-v2, in an even further fashion than presently modeled (see Section 4.2). Capital breeding being the dominant reproductive strategy for marine copepods in regions characterized by strong seasonality (Sainmont et al., 2014), implementing this strategy in PISCES-MOG would alter our results. In this case, the impact of reproduction and ontogenetic growth on mesozooplankton seasonality and on metazoan-driven carbon export seasonal dynamics would be higher than currently simulated in high latitude regions.

Another caveat is that our model misses part of the complex processes through which mesozooplankton interact with the BCP (Steinberg & Landry, 2017). In particular, (Boyd et al., 2019) estimated the contribution of five additional mechanisms to the gravitational carbon pump, referred to as "particle injection pumps." Two of these mechanisms are directly linked to zooplankton: (a) the mortality of specific zooplankton groups undertaking seasonal migration to hibernate in the deep ocean (the "seasonal lipid pump," Jónasdóttir et al., 2015; Pinti, DeVries et al., 2023), and (b) the active transport of organic carbon by organisms that feed in surface layers and excrete in deeper layers by performing DVM (the "mesopelagic-migrant pump"). As a result, the gravitational pump alone exports between 4 and 9 PgC yr^{-1}, whereas incorporating the "particle injection pumps" would increase this export flux up to 5 to 16 PgC yr^{-1} (Boyd et al., 2019). Notably, DVM alone would contribute several petagrams of carbon per year (Aumont et al., 2018; Boyd et al., 2019; Pinti, Jónasdóttir, et al., 2023). Thus, in a

model also accounting for both migration (i.e., DVM and hibernation) and reproduction processes, representing DVM and hibernation would increase the export of particles whereas reproduction would decrease it (see Section 3.3.3). Yet, it remains difficult to hypothesize how the combination of these two processes would impact total export, since they have opposing effects on these fluxes. So far, these processes have been evaluated independently in different models (Aumont et al., 2018; Jónasdóttir et al., 2015), including ours, but no global biogeochemical model currently integrates all these processes in its representation of zooplankton. The ongoing developments in zooplankton observation systems (Irisson et al., 2022; Lombard et al., 2019) and the emergence of more spatially explicit data products of group-specific plankton biomass (Drago et al., 2022; Knecht et al., 2023) will facilitate the development of such integrative models and they will help to better constrain BCP estimates in a context of climate change.

5. Conclusions

Our study provides new insights into the impact of a more realistic representation of mesozooplankton biology on community structure, plankton functional type dynamics, and the export of organic carbon to depth in a global model. The inclusion of ontogenetic growth and reproduction shifts the structure of the zooplankton community toward smaller organisms (more mesozooplankton, less microzooplankton) and thus toward smaller organic particles, compared to that simulated by a model with a single and nonvarying size representation (as in PISCES-v2). This shift increases the grazing pressure on the nanophytoplankton while relaxing it for larger phytoplankton (diatoms), thus influencing the structure of the phytoplankton community size inversely to that of zooplankton. The net effect of mesozooplankton ontogeny and reproduction on total particles is a shift toward smaller particles, significantly reducing organic carbon export below 100 m depth compared to a previous version of PISCES. This suggests that including ontogeny and reproduction would increase the contribution of zooplankton to the Biological Carbon Pump (BCP) export in many biogeochemical components of Earth System Models (ESMs).

Surprisingly, despite the partial representation of zooplankton life histories in our model that induced cohort dynamics, the emergent impact of this representation on the phenology of living ecosystem and non-living particle components is limited, even though it was important for their mean annual distribution. However, we could benefit from the cohort behavior that emerges in PISCES-MOG to improve the understanding of zooplankton-driven carbon flux dynamics and BCP seasonality. This would require new model developments, such as incorporating mesozooplankton capital breeding at high latitude or representing the size spectrum of non-living particles and could be the subject of further studies.

We emphasize that the observations-based mesozooplankton biomass climatology provide valuable insights into the seasonal patterns of global zooplankton biomass as they unlock spatial and temporal scales that were not covered by the previous observations. New model development and data-based product presented in this study contribute to improve model-observation synergies to understand the role of mesozooplankton on the biological carbon pump, and to characterize the level of abstraction necessary to accurately estimate its contribution to carbon fluxes.

Finally, here, we focused of the biogeochemical impacts of the mesozooplankton reproduction and ontogenetic growth. Given that mesozooplankton serve as food for many predators, understanding their life cycles and ontogenetic growth could also regulate the dynamics of higher trophic levels. Therefore, it would be relevant to study the effects of these characteristics in a model explicitly representing the top of the trophic chain, for example, APECOSM (Dupont et al., 2023; Maury, 2010). In particular, the size structure of zooplanktivorous predators could be influenced by the cohort pattern. Smaller predators would be favored at the beginning of the cohort when smaller metazoans dominate, while larger ones would emerge later along with larger metazoans.

Conflict of Interest

The authors declare no conflicts of interest relevant to this study.

Data Availability Statement

The codes, data sets and model outputs needed to reproduce the figures, are openly available in Zenodo (Clerc, 2024).

Acknowledgments
All simulations have been performed on the computing center Datarmor operated by the Pôle de Calcul et de Données pour la Mer in Brest, France. This also study benefited from the ESPRI (Ensemble de Services Pour la Recherche l'IPSL) computing and data center (https://mesocentre.ipsl.fr, last accessed 28 February 2024), which is supported by CNRS, Sorbonne Université, Ecole Polytechnique, and CNES and through national and international grants. This study has received funding from the European Union's Horizon 2020 Research and Innovation Programme, under Grant 101094227 (Blue-Cloud2026), under Grant 862923 (AtlantECO) and under Grant 101059915 (BIOceans5D). This output reflects only the author's view, and the European Union cannot be held responsible for any use that may be made of the information contained therein. Laurent Bopp acknowledges support from the European Union's Horizon 2020 research and innovation ESM2025 (Grant 101003536), from the project VESRI-CALIPSO and from the Chaire ENS-Chanel. Open access funding provided by Eidgenossische Technische Hochschule Zurich.

References

Andersen, K. H., Berge, T., Gonçalves, R. J., Hartvig, M., Heuschele, J., Hylander, S., et al. (2016). Characteristic sizes of life in the oceans, from bacteria to whales. *Annual Review of Marine Science*, *8*(1), 217–241. https://doi.org/10.1146/annurev-marine-122414-034144

Aumont, O., Ethé, C., Tagliabue, A., Bopp, L., & Gehlen, M. (2015). PISCES-v2: An ocean biogeochemical model for carbon and ecosystem studies. *Geoscientific Model Development*, *8*(8), 2465–2513. https://doi.org/10.5194/gmd-8-2465-2015

Aumont, O., Maury, O., Lefort, S., & Bopp, L. (2018). Evaluating the potential impacts of the diurnal vertical migration by marine organisms on marine biogeochemistry. *Global Biogeochemical Cycles*, *32*(11), 1622–1643. https://doi.org/10.1029/2018gb005886

Baird, M. E., & Suthers, I. M. (2007). A size-resolved pelagic ecosystem model. *Ecological Modelling*, *203*(3–4), 185–203. https://doi.org/10.1016/j.ecolmodel.2006.11.025

Basedow, S. L., McKee, D., Lefering, I., Gislason, A., Daase, M., Trudnowska, E., et al. (2019). Remote sensing of zooplankton swarms. *Scientific Reports*, *9*(1), 686. https://doi.org/10.1038/s41598-018-37129-x

Baumgartner, M. F., & Tarrant, A. M. (2017). The physiology and ecology of diapause in marine copepods. *Annual Review of Marine Science*, *9*(1), 387–411. https://doi.org/10.1146/annurev-marine-010816-060505

Bell, D. M., & Schlaepfer, D. R. (2016). On the dangers of model complexity without ecological justification in species distribution modeling. *Ecological Modelling*, *330*, 50–59. https://doi.org/10.1016/j.ecolmodel.2016.03.012

Benedetti, F., Gruber, N., & Vogt, M. (2023). Global gradients in species richness of marine plankton functional groups. *Journal of Plankton Research*, *45*(6), 832–852. https://doi.org/10.1093/plankt/fbad044

Benedetti, F., Vogt, M., Elizondo, U. H., Righetti, D., Zimmermann, N. E., & Gruber, N. (2021). Major restructuring of marine plankton assemblages under global warming. *Nature Communications*, *12*(1), 5226. https://doi.org/10.1038/s41467-021-25385-x

Blanchard, J. L., Andersen, K. H., Scott, F., Hintzen, N. T., Piet, G., & Jennings, S. (2014). Evaluating targets and trade-offs among fisheries and conservation objectives using a multispecies size spectrum model. *Journal of Applied Ecology*, *51*(3), 612–622. https://doi.org/10.1111/1365-2664.12238

Boyd, P. W., Claustre, H., Levy, M., Siegel, D. A., & Weber, T. (2019). Multi-faceted particle pumps drive carbon sequestration in the ocean. *Nature*, *568*(7752), 327–335. https://doi.org/10.1038/s41586-019-1098-2

Brun, P., Kiørboe, T., Licandro, P., & Payne, M. R. (2016). The predictive skill of species distribution models for plankton in a changing climate. *Global Change Biology*, *22*(9), 3170–3181. https://doi.org/10.1111/gcb.13274

Brun, P., Payne, M. R., & Kiørboe, T. (2017). A trait database for marine copepods. *Earth System Science Data*, *9*(1), 99–113. https://doi.org/10.5194/essd-9-99-2017

Buitenhuis, E., Le Quéré, C., Aumont, O., Beaugrand, G., Bunker, A., Hirst, A., et al. (2006). Biogeochemical fluxes through mesozooplankton. *Global Biogeochemical Cycles*, *20*(2). https://doi.org/10.1029/2005gb002511

Cael, B., Cavan, E. L., & Britten, G. L. (2021). Reconciling the size-dependence of marine particle sinking speed. *Geophysical Research Letters*, *48*(5), e2020GL091771. https://doi.org/10.1029/2020gl091771

Calbet, A. (2001). Mesozooplankton grazing effect on primary production: A global comparative analysis in marine ecosystems. *Limnology & Oceanography*, *46*(7), 1824–1830. https://doi.org/10.4319/lo.2001.46.7.1824

Chust, G., Allen, J. I., Bopp, L., Schrum, C., Holt, J., Tsiaras, K., et al. (2014). Biomass changes and trophic amplification of plankton in a warmer ocean. *Global Change Biology*, *20*(7), 2124–2139. https://doi.org/10.1111/gcb.12562

Clements, D., Yang, S., Weber, T., McDonnell, A., Kiko, R., Stemmann, L., & Bianchi, D. (2023). New estimate of organic carbon export from optical measurements reveals the role of particle size distribution and export horizon. *Global Biogeochemical Cycles*, *37*(3), e2022GB007633. https://doi.org/10.1029/2022gb007633

Clerc, C. (2024). Supplementary materials for "Effects of mesozooplankton growth and reproduction on plankton and organic carbon dynamics in a marine biogeochemical model". *Zenodo*. https://doi.org/10.5281/zenodo.12166409

Clerc, C., Aumont, O., & Bopp, L. (2021). Should we account for mesozooplankton reproduction and ontogenetic growth in biogeochemical modeling? *Theoretical Ecology*, *14*(4), 589–609. https://doi.org/10.1007/s12080-021-00519-5

Clerc, C., Aumont, O., & Bopp, L. (2023). Filter-feeding gelatinous macrozooplankton response to climate change and implications for benthic food supply and global carbon cycle. *Global Change Biology*, *29*(22), 6383–6398. https://doi.org/10.1111/gcb.16942

Clerc, C., Bopp, L., Benedetti, F., Vogt, M., & Aumont, O. (2023). Including filter-feeding gelatinous macrozooplankton in a global marine biogeochemical model: Model–data comparison and impact on the ocean carbon cycle. *Biogeosciences*, *20*(4), 869–895. https://doi.org/10.5194/bg-20-869-2023

Datta, S., & Blanchard, J. L. (2016). The effects of seasonal processes on size spectrum dynamics. *Canadian Journal of Fisheries and Aquatic Sciences*, *73*(4), 598–610. https://doi.org/10.1139/cjfas-2015-0468

De Roos, A. M., & Persson, L. (2003). Competition in size-structured populations: Mechanisms inducing cohort formation and population cycles. *Theoretical Population Biology*, *63*(1), 1–16. https://doi.org/10.1016/S0040-5809(02)00009-6

De Roos, A. M., Schellekens, T., Van Kooten, T., Van De Wolfshaar, K., Claessen, D., & Persson, L. (2008). Simplifying a physiologically structured population model to a stage-structured biomass model. *Theoretical Population Biology*, *73*(1), 47–62. https://doi.org/10.1016/j.tpb.2007.09.004

DeVries, T., & Weber, T. (2017). The export and fate of organic matter in the ocean: New constraints from combining satellite and oceanographic tracer observations. *Global Biogeochemical Cycles*, *31*(3), 535–555. https://doi.org/10.1002/2016gb005551

Dormann, C. F., Elith, J., Bacher, S., Buchmann, C., Carl, G., Carré, G., et al. (2013). Collinearity: A review of methods to deal with it and a simulation study evaluating their performance. *Ecography*, *36*(1), 27–46. https://doi.org/10.1111/j.1600-0587.2012.07348.x

Drago, L., Panaïotis, T., Irisson, J.-O., Babin, M., Biard, T., Carlotti, F., et al. (2022). Global distribution of zooplankton biomass estimated by in situ imaging and machine learning. *Frontiers in Marine Science*, *9*. https://doi.org/10.3389/fmars.2022.894372

Druon, J.-N., Hélaouët, P., Beaugrand, G., Fromentin, J.-M., Palialexis, A., & Hoepffner, N. (2019). Satellite-based indicator of zooplankton distribution for global monitoring. *Scientific Reports*, *9*(1), 4732. https://doi.org/10.1038/s41598-019-41212-2

Ducklow, H. W., & Harris, R. P. (1993). Introduction to the JGOFS north Atlantic bloom experiment. *Deep Sea Research Part II: Topical Studies in Oceanography*, *40*(1–2), 1–8. https://doi.org/10.1016/0967-0645(93)90003-6

Dupont, L., Le Mézo, P., Aumont, O., Bopp, L., Clerc, C., Ethé, C., & Maury, O. (2023). High trophic level feedbacks on global ocean carbon uptake and marine ecosystem dynamics under climate change. *Global Change Biology*, *29*(6), 1545–1556. https://doi.org/10.1111/gcb.16558

Elith, J., Kearney, M., & Phillips, S. (2010). The art of modelling range-shifting species. *Methods in Ecology and Evolution*, *1*(4), 330–342. https://doi.org/10.1111/j.2041-210x.2010.00036.x

Elith, J., & Leathwick, J. R. (2009). Species distribution models: Ecological explanation and prediction across space and time. *Annual Review of Ecology Evolution and Systematics*, *40*(1), 677–697. https://doi.org/10.1146/annurev.ecolsys.110308.120159

Eyring, V., Bony, S., Meehl, G. A., Senior, C. A., Stevens, B., Stouffer, R. J., & Taylor, K. E. (2016). Overview of the coupled model intercomparison project phase 6 (CMIP6) experimental design and organization. *Geoscientific Model Development*, *9*(5), 1937–1958. https://doi.org/10.5194/gmd-9-1937-2016

Field, C. B., Behrenfeld, M. J., Randerson, J. T., & Falkowski, P. (1998). Primary production of the biosphere: Integrating terrestrial and oceanic components. *Science*, *281*(5374), 237–240. https://doi.org/10.1126/science.281.5374.237

Guisan, A., & Zimmermann, N. E. (2000). Predictive habitat distribution models in ecology. *Ecological Modelling*, *135*(2–3), 147–186. https://doi.org/10.1016/S0304-3800(00)00354-9

Hansen, P. J., BjØrnsen, P. K., & Hansen, B. W. (1997). Zooplankton grazing and growth: Scaling within the 2-2,000-µm body size range. *Limnology & Oceanography*, *42*(4), 687–704. https://doi.org/10.4319/lo.1997.42.4.0687

Hartvig, M., Andersen, K. H., & Beyer, J. E. (2011). Food web framework for size-structured populations. *Journal of Theoretical Biology*, *272*(1), 113–122. https://doi.org/10.1016/j.jtbi.2010.12.006

Hatton, I. A., Heneghan, R. F., Bar-On, Y. M., & Galbraith, E. D. (2021). The global ocean size spectrum from bacteria to whales. *Science Advances*, *7*(46), eabh3732. https://doi.org/10.1126/sciadv.abh3732

Hébert, M.-P., Beisner, B. E., & Maranger, R. (2017). Linking zooplankton communities to ecosystem functioning: Toward an effect-trait framework. *Journal of Plankton Research*, *39*(1), 3–12. https://doi.org/10.1093/plankt/fbw068

Heneghan, R. F., Everett, J. D., Sykes, P., Batten, S. D., Edwards, M., Takahashi, K., et al. (2020). A functional size-spectrum model of the global marine ecosystem that resolves zooplankton composition. *Ecological Modelling*, *435*, 109265. https://doi.org/10.1016/j.ecolmodel.2020.109265

Hirche, H.-J. (1996). Diapause in the marine copepod, calanus finmarchicus—A review. *Ophelia*, *44*(1–3), 129–143. https://doi.org/10.1080/00785326.1995.10429843

Irisson, J.-O., Ayata, S.-D., Lindsay, D. J., Karp-Boss, L., & Stemmann, L. (2022). Machine learning for the study of plankton and marine snow from images. *Annual Review of Marine Science*, *14*(1), 277–301. https://doi.org/10.1146/annurev-marine-041921-013023

Jackson, G. A. (1993). Flux feeding as a mechanism for zooplankton grazing and its implications for vertical particulate flux 1. *Limnology & Oceanography*, *38*(6), 1328–1331. https://doi.org/10.4319/lo.1993.38.6.1328

Jammalamadaka, S. R., & SenGupta, A. (2001). *Topics in circular statistics* (Vol. 5). World Scientific. https://doi.org/10.1142/4031

Jónasdóttir, S. H., Visser, A. W., Richardson, K., & Heath, M. R. (2015). Seasonal copepod lipid pump promotes carbon sequestration in the deep north Atlantic. *Proceedings of the National Academy of Sciences*, *112*(39), 12122–12126. https://doi.org/10.1073/pnas.1512110112

Kearney, K. A., Bograd, S. J., Drenkard, E., Gomez, F. A., Haltuch, M., Hermann, A. J., et al. (2021). Using global-scale earth system models for regional fisheries applications. *Frontiers in Marine Science*, *8*, 622206. https://doi.org/10.3389/fmars.2021.622206

Kenitz, K. M., Visser, A. W., Mariani, P., & Andersen, K. H. (2017). Seasonal succession in zooplankton feeding traits reveals trophic trait coupling. *Limnology & Oceanography*, *62*(3), 1184–1197. https://doi.org/10.1002/lno.10494

Kiørboe, T. (2011). How zooplankton feed: Mechanisms, traits and trade-offs. *Biological Reviews*, *86*(2), 311–339. https://doi.org/10.1111/j.1469-185x.2010.00148.x

Kiørboe, T., Visser, A., & Andersen, K. H. (2018). A trait-based approach to ocean ecology. *ICES Journal of Marine Science*, *75*(6), 1849–1863. https://doi.org/10.1093/icesjms/fsy090

Knecht, N. S., Benedetti, F., Hofmann Elizondo, U., Bednaršek, N., Chaabane, S., de Weerd, C., et al. (2023). The impact of zooplankton calcifiers on the marine carbon cycle. *Global Biogeochemical Cycles*, *37*(6), e2022GB007685. https://doi.org/10.1029/2022gb007685

Kooijman, S. (2013). Waste to hurry: Dynamic energy budgets explain the need of wasting to fully exploit blooming resources. *Oikos*, *122*(3), 348–357. https://doi.org/10.1111/j.1600-0706.2012.00098.x

Kwiatkowski, L., Aumont, O., & Bopp, L. (2019). Consistent trophic amplification of marine biomass declines under climate change. *Global Change Biology*, *25*(1), 218–229. https://doi.org/10.1111/gcb.14468

Le Quéré, C., Harrison, S. P., Colin Prentice, I., Buitenhuis, E. T., Aumont, O., Bopp, L., et al. (2005). Ecosystem dynamics based on plankton functional types for global ocean biogeochemistry models. *Global Change Biology*, *11*(11), 2016–2040. https://doi.org/10.1111/j.1365-2486.2005.1004.x

Litchman, E., Ohman, M. D., & Kiørboe, T. (2013). Trait-based approaches to zooplankton communities. *Journal of Plankton Research*, *35*(3), 473–484. https://doi.org/10.1093/plankt/fbt019

Llort, J., Lévy, M., Sallée, J.-B., & Tagliabue, A. (2015). Onset, intensification, and decline of phytoplankton blooms in the southern ocean. *ICES Journal of Marine Science*, *72*(6), 1971–1984. https://doi.org/10.1093/icesjms/fsv053

Lombard, F., Boss, E., Waite, A. M., Vogt, M., Uitz, J., Stemmann, L., et al. (2019). Globally consistent quantitative observations of planktonic ecosystems. *Frontiers in Marine Science*, *6*, 196. https://doi.org/10.3389/fmars.2019.00196

Luo, J. Y., Stock, C. A., Henschke, N., Dunne, J. P., & O'Brien, T. D. (2022). Global ecological and biogeochemical impacts of pelagic tunicates. *Progress in Oceanography*, *205*, 102822. https://doi.org/10.1016/j.pocean.2022.102822

Mackas, D., Greve, W., Edwards, M., Chiba, S., Tadokoro, K., Eloire, D., et al. (2012). Changing zooplankton seasonality in a changing ocean: Comparing time series of zooplankton phenology. *Progress in Oceanography*, *97*, 31–62. https://doi.org/10.1016/j.pocean.2011.11.005

Madec, G. (2008). Nemo reference manual, ocean dynamic component: Nemo–opa, note du pôle de modélisation, institut pierre simon laplace (Tech. Rep.). Technical Report 27, Note du pôle de modélisation, Institut Pierre Simmon ….

Madin, L. P., Horgan, E. F., & Steinberg, D. K. (2001). Zooplankton at the Bermuda Atlantic time-series study (bats) station: Diel, seasonal and interannual variation in biomass, 1994–1998. *Deep Sea Research Part II: Topical Studies in Oceanography*, *48*(8–9), 2063–2082. https://doi.org/10.1016/s0967-0645(00)00171-5

Mauchline, J. (1998). Adv. mar. biol. 33: The biology of calanoid copepods.

Maury, O. (2010). An overview of APECOSM, a spatialized mass balanced "Apex Predators ECOSystem Model" to study physiologically structured tuna population dynamics in their ecosystem. *Progress in Oceanography*, *84*(1–2), 113–117. https://doi.org/10.1016/j.pocean.2009.09.013

Maury, O., Faugeras, B., Shin, Y.-J., Poggiale, J.-C., Ari, T. B., & Marsac, F. (2007). Modeling environmental effects on the size-structured energy flow through marine ecosystems. Part 1: The model. *Progress in Oceanography*, *74*(4), 479–499. https://doi.org/10.1016/j.pocean.2007.05.002

McCauley, E., & Murdoch, W. W. (1987). Cyclic and stable populations: Plankton as paradigm. *The American Naturalist*, *129*(1), 97–121. https://doi.org/10.1086/284624

Melo-Merino, S. M., Reyes-Bonilla, H., & Lira-Noriega, A. (2020). Ecological niche models and species distribution models in marine environments: A literature review and spatial analysis of evidence. *Ecological Modelling*, *415*, 108837. https://doi.org/10.1016/j.ecolmodel.2019.108837

Mitra, A., Caron, D. A., Faure, E., Flynn, K. J., Leles, S. G., Hansen, P. J., et al. (2023). The Mixoplankton Database (MDB): Diversity of photo-phago-trophic plankton in form, function, and distribution across the global ocean. *Journal of Eukaryotic Microbiology*, *70*(4), e12972. https://doi.org/10.1111/jeu.12972

Moriarty, R., & O'Brien, T. (2013). Distribution of mesozooplankton biomass in the global ocean. *Earth System Science Data*, *5*(1), 45–55. https://doi.org/10.5194/essd-5-45-2013

Nash, J. E., & Sutcliffe, J. V. (1970). River flow forecasting through conceptual models Part I—A discussion of principles. *Journal of Hydrology*, *10*(3), 282–290. https://doi.org/10.1016/0022-1694(70)90255-6

O'Brien, T. D. (2005). COPEPOD, a global plankton database: A review of the 2005 database contents and creation of new global zooplankton biomass fields. Retrieved from https://repository.library.noaa.gov/view/noaa/3497/noaa_3497_DS1.pdf

O'Brien, T. D. (2010). Copepod, a global plankton database: A review of the 2010 database contents, processing methods, and access interface. Retrieved from https://repository.library.noaa.gov/view/noaa/5040/noaa_5040_DS1.pdf

Orenstein, E. C., Ayata, S.-D., Maps, F., Becker, É. C., Benedetti, F., Biard, T., et al. (2022). Machine learning techniques to characterize functional traits of plankton from image data. *Limnology & Oceanography*, *67*(8), 1647–1669. https://doi.org/10.1002/lno.12101

Persson, L., & de Roos, A. M. (2013). Symmetry breaking in ecological systems through different energy efficiencies of juveniles and adults. *Ecology*, *94*(7), 1487–1498. https://doi.org/10.1890/12-1883.1

Persson, L., Leonardsson, K., De Roos, A. M., Gyllenberg, M., & Christensen, B. (1998). Ontogenetic scaling of foraging rates and the dynamics of a size-structured consumer-resource model. *Theoretical Population Biology*, *54*(3), 270–293. https://doi.org/10.1006/tpbi.1998.1380

Picheral, M., Catalano, C., Brousseau, D., Claustre, H., Coppola, L., Leymarie, E., et al. (2022). The underwater vision profiler 6: An imaging sensor of particle size spectra and plankton, for autonomous and cabled platforms. *Limnology and Oceanography: Methods*, *20*(2), 115–129. https://doi.org/10.1002/lom3.10475

Pinti, J., DeVries, T., Norin, T., Serra-Pompei, C., Proud, R., Siegel, D. A., et al. (2023). Model estimates of metazoans' contributions to the biological carbon pump. *Biogeosciences*, *20*(5), 997–1009. https://doi.org/10.5194/bg-20-997-2023

Pinti, J., Jónasdóttir, S. H., Record, N. R., & Visser, A. W. (2023). The global contribution of seasonally migrating copepods to the biological carbon pump. *Limnology & Oceanography*, *68*(5), 1147–1160. https://doi.org/10.1002/lno.12335

Pope, J. G., Shepherd, J. G., Webb, J., Stebbing, A. R. D., Mangel, M., Beverton, R. J. H., et al. (1994). Successful surf-riding on size spectra: The secret of survival in the sea. *Philosophical Transactions of the Royal Society of London - Series B: Biological Sciences*, *343*(1303), 41–49. https://doi.org/10.1098/rstb.1994.0006

Qiao, H., Feng, X., Escobar, L. E., Peterson, A. T., Soberón, J., Zhu, G., & Papeş, M. (2019). An evaluation of transferability of ecological niche models. *Ecography*, *42*(3), 521–534. https://doi.org/10.1111/ecog.03986

Quevedo, M., & Anadón, R. (2000). Spring microzooplankton composition, biomass and potential grazing in the central Cantabrian coast (southern Bay of Biscay). *Oceanologica Acta*, *23*(3), 297–310. https://doi.org/10.1016/S0399-1784(00)00128-6

R Core Team. (2022). R: A language and environment for statistical computing. [Computer software manual]. https://www.R-project.org/

Righetti, D., Vogt, M., Gruber, N., Psomas, A., & Zimmermann, N. E. (2019). Global pattern of phytoplankton diversity driven by temperature and environmental variability. *Science Advances*, *5*(5), eaau6253. https://doi.org/10.1126/sciadv.aau6253

Rohr, T., Richardson, A. J., Lenton, A., Chamberlain, M. A., & Shadwick, E. H. (2023). Zooplankton grazing is the largest source of uncertainty for marine carbon cycling in cmip6 models. *Communications Earth & Environment*, *4*(1), 212. https://doi.org/10.1038/s43247-023-00871-w

Romagnan, J.-B., Legendre, L., Guidi, L., Jamet, J.-L., Jamet, D., Mousseau, L., et al. (2015). Comprehensive model of annual plankton succession based on the whole-plankton time series approach. *PLoS One*, *10*(3), e0119219. https://doi.org/10.1371/journal.pone.0119219

Safi, K. A., Brian Griffiths, F., & Hall, J. A. (2007). Microzooplankton composition, biomass and grazing rates along the WOCE SR3 line between Tasmania and Antarctica. *Deep Sea Research Part I: Oceanographic Research Papers*, *54*(7), 1025–1041. https://doi.org/10.1016/J.DSR.2007.05.003

Sainmont, J., Andersen, K. H., Varpe, Ø., & Visser, A. W. (2014). Capital versus income breeding in a seasonal environment. *The American Naturalist*, *184*(4), 466–476. https://doi.org/10.1086/677926

Serra-Pompei, C., Soudijn, F., Visser, A. W., Kiørboe, T., & Andersen, K. H. (2020). A general size-and trait-based model of plankton communities. *Progress in Oceanography*, *189*, 102473. https://doi.org/10.1016/j.pocean.2020.102473

Serra-Pompei, C., Ward, B. A., Pinti, J., Visser, A. W., Kiørboe, T., & Andersen, K. H. (2022). Linking plankton size spectra and community composition to carbon export and its efficiency. *Global Biogeochemical Cycles*, *36*(5), e2021GB007275. https://doi.org/10.1029/2021gb007275

Sheldon, R. W., Prakash, A., & Sutcliffe, W. H. (1972). The size distribution of particles in the ocean. *Limnology & Oceanography*, *17*(3), 327–340. https://doi.org/10.4319/lo.1972.17.3.0327

Sheridan, C. C., & Landry, M. R. (2004). A 9-year increasing trend in mesozooplankton biomass at the Hawaii ocean time-series station aloha. *ICES Journal of Marine Science*, *61*(4), 457–463. https://doi.org/10.1016/j.icesjms.2004.03.023

Siegel, D., Buesseler, K., Doney, S. C., Sailley, S., Behrenfeld, M. J., & Boyd, P. (2014). Global assessment of ocean carbon export by combining satellite observations and food-web models. *Global Biogeochemical Cycles*, *28*(3), 181–196. https://doi.org/10.1002/2013gb004743

Sprules, W. G., & Barth, L. E. (2016). Surfing the biomass size spectrum: Some remarks on history, theory, and application. *Canadian Journal of Fisheries and Aquatic Sciences*, *73*(4), 477–495. https://doi.org/10.1139/cjfas-2015-0115

Steinberg, D. K., Carlson, C. A., Bates, N. R., Johnson, R. J., Michaels, A. F., & Knap, A. H. (2001). Overview of the US JGOFS Bermuda Atlantic time-series study (bats): A decade-scale look at ocean biology and biogeochemistry. *Deep Sea Research Part II: Topical Studies in Oceanography*, *48*(8–9), 1405–1447. https://doi.org/10.1016/s0967-0645(00)00148-x

Steinberg, D. K., & Landry, M. R. (2017). Zooplankton and the ocean carbon cycle. *Annual Review of Marine Science*, *9*(1), 413–444. https://doi.org/10.1146/annurev-marine-010814-015924

Stock, C. A., Dunne, J. P., & John, J. G. (2014). Global-scale carbon and energy flows through the marine planktonic food web: An analysis with a coupled physical–biological model. *Progress in Oceanography*, *120*, 1–28. https://doi.org/10.1016/j.pocean.2013.07.001

Strömberg, K. P., Smyth, T. J., Allen, J. I., Pitois, S., & O'Brien, T. D. (2009). Estimation of global zooplankton biomass from satellite ocean colour. *Journal of Marine Systems*, *78*(1), 18–27. https://doi.org/10.1016/j.jmarsys.2009.02.004

Stukel, M. R., Ohman, M. D., Kelly, T. B., & Biard, T. (2019). The roles of suspension-feeding and flux-feeding zooplankton as gatekeepers of particle flux into the mesopelagic ocean in the northeast pacific. *Frontiers in Marine Science*, *397*. https://doi.org/10.3389/fmars.2019.00397

Taylor, K. E., Stouffer, R. J., & Meehl, G. A. (2012). An overview of cmip5 and the experiment design. *Bulletin of the American Meteorological Society*, *93*(4), 485–498. https://doi.org/10.1175/bams-d-11-00094.1

Varpe, Ø., Jørgensen, C., Tarling, G. A., & Fiksen, Ø. (2009). The adaptive value of energy storage and capital breeding in seasonal environments. *Oikos*, *118*(3), 363–370. https://doi.org/10.1111/j.1600-0706.2008.17036.x

Waldock, C., Stuart-Smith, R. D., Albouy, C., Cheung, W. W., Edgar, G. J., Mouillot, D., et al. (2022). A quantitative review of abundance-based species distribution models. *Ecography*, *2022*(1). https://doi.org/10.1111/ecog.05694

Westberry, T. K., Silsbe, G. M., & Behrenfeld, M. J. (2023). Gross and net primary production in the global ocean: An ocean color remote sensing perspective. *Earth-Science Reviews*, *237*, 104322. https://doi.org/10.1016/j.earscirev.2023.104322

Wright, R. M., Le Quéré, C., Buitenhuis, E., Pitois, S., & Gibbons, M. J. (2021). Role of jellyfish in the plankton ecosystem revealed using a global ocean biogeochemical model. *Biogeosciences*, *18*(4), 1291–1320. https://doi.org/10.5194/bg-18-1291-2021

Zhou, M., Carlotti, F., & Zhu, Y. (2010). A size-spectrum zooplankton closure model for ecosystem modelling. *Journal of Plankton Research*, *32*(8), 1147–1165. https://doi.org/10.1093/plankt/fbq054